# The polycomb repressor complex 2 and Enhancer of Zeste 2 regulate glial reactivity and are required for the formation of Müller glia-derived progenitor cells in the retina

Warren A. Campbell[1#], Heithem M. El-Hodiri [1#], Diego Torres [1], Evan C. Hawthorn [1], Lisa E. Kelly [1], Leo Volkov [2], David Akanonu [3], and Andy J. Fischer[1*]

1 Department of Neuroscience, College of Medicine, The Ohio State University, Columbus, OH

2 Department of Pathology and Immunology, Washington University School of Medicine, St. Louis, MO.

3 Neuroscience Graduate Program, University of Michigan, Ann Arbor, MI.

# these authors contributed equally

***corresponding author**: Andy J. Fischer, Department of Neuroscience, Ohio State University, College of Medicine, 3020 Graves Hall, 333 W. 10th Ave, Columbus, OH 43210-1239, USA. Telephone: (614) 292-3524; Fax: (614) 688-8742; email: Andrew.Fischer@osumc.edu

**Abbreviated title**: EZH2 and PRC2 in Müller glia and Müller glia-derived progenitor cells

**Number of pages**: 74 **Number of Figures**: 11 **Number of Supplemental Figures**: 4 **Number of Tables:** 1 **Number of Supplemental Tables**: 3

**Author Contributions:** WAC, HE-H and LV designed and executed experiments, gathered data, constructed figures and contributed to writing the manuscript. DT, EH, LK and DA executed experiments and gathered data. AJF designed experiments, analyzed data, constructed figures and wrote the manuscript.

**Acknowledgements:** This work was supported by RO1 EY022030-10 (AJF).

**Abstract:** EZH2 (Enhancer of Zeste 2), a key component of the Polycomb Repressor Complex 2 (PRC2), is required for the differentiation of Müller glia (MG) during retinal development. However, nothing is known about the roles of EZH2 and PRC2 in mature or damaged retinas. Herein, we investigate the expression of PRC2-related factors and roles during the formation of Müller glia-derived progenitor cells (MGPCs) in the chick and mouse retinas. In chick, *EZH2,* PRC2-related factors, and EZH2-activators, *JARID2* and *AEBP1*, are dynamically expressed by MG and MGPCs in damaged retinas. Inhibition of EZH2, EED or JARID2 blocks the formation of MGPCs. Similarly, inhibition of EZH2 suppresses the proliferation of progenitors in the circumferential marginal zone. By using a combination of single cell RNA-seq and single cell ATAC-seq, we find significant changes in gene expression and chromatin access in MG with EZH2 inhibition and NMDA-treatment, and many of these genes are associated with glial and neuronal differentiation. Correlation across gene expression, chromatin access and transcription factor motif access in MG was observed for transcription factors known to covey glial identity and promote retinal development. In the mouse retina, components of the PRC2 complex are downregulated in MG in damaged retinas and inhibition of EZH2 has no effect upon the formation of neuron-like cells from Ascl1-overexpressing MG. We conclude that in the chick, but not mouse, the activity of EZH2 is required for the reprogramming of MG into MGPCs by regulating chromatin access to transcription factors associated with glial differentiation and retinal development.

## Introduction:

Müller glia (MG) are the predominant support cells in the retina and are common to all vertebrate classes. MG perform many important functions including structural support, synaptic support, osmotic homeostasis, and metabolic support to retinal neurons (Bringmann et al., 2006; Bringmann et al., 2009). However, MG also have the extraordinary capability to de-differentiate, proliferate, acquire a progenitor phenotype, and generate new neurons (Bernardos et al., 2007; Fausett et al., 2008; Fischer and Reh, 2001; Karl et al., 2008; Ooto et al., 2004). The transition of MG to Müller glia-derived progenitor cells (MGPCs) involves downregulation of glial genes, upregulation of progenitor-associated factors and proliferation followed by neuronal differentiation (Fischer and Bongini, 2010; Gallina et al., 2014a; Todd and Reh, 2021; Wilken and Reh, 2016). The process of retinal regeneration is efficient in fish, whereas this process is ineffective in mammals. By comparison, the process of retinal regeneration in birds is limited; numerous proliferating MGPCs are formed, but few of the progeny differentiate into neurons (Gallina et al., 2014a). Accordingly, the chick represents a valuable model in which to study factors that activate or suppress the formation of neurogenic MGPCs.

The formation of MGPCs can be stimulated by severe acute retinal damage, however MGPCs can also be generated without inducing neuronal death. In chick retina, consecutive daily injections of Fibroblast Growth Factor 2 (FGF2) and/or insulin/IGF1 activate cell-signaling networks to stimulate the formation of MGPCs (Fischer et al., 2002b; Fischer et al., 2014a). In zebrafish retina, activation of Wnt-signaling or MAPK-signaling via HB-EGF or FGF2+insulin can stimulate the formation of MGPCs and *de novo* neurogenesis (Ramachandran et al., 2011a; Wan et al., 2012a;

Zhao et al., 2014). Further, TNFα combined with Notch-inhibitor is sufficient to stimulate the formation of MGPCs and *de novo* neurogenesis in zebrafish retina (Conner et al., 2014; Nelson et al., 2013). In mouse retina, significant stimulation is required to induce the formation of MGPCs. For example, the forced expression of the transcription factor *Ascl1*, in combination with NMDA-induced damage and inhibition of Histone Deacetylases (HDACs), stimulates reprogramming of MG into functional, light-responsive neurons (Jorstad et al., 2017; Pollak et al., 2013; Ueki et al., 2015). The differentiation of neurons from *Ascl1* over-expressing MG can be enhanced by ablating reactive microglia (Todd et al., 2020), inhibiting Jak/Stat-signaling (Jorstad et al., 2020), NFkB-signaling, TGFβ/Smad3-signaling or ID transcription factors (Palazzo et al., 2021), or combined over-expression of *Ascl1* with *Atoh1* (Todd et al., 2021).

The purpose of this study was to investigate how the activity of EZH2 regulates the dedifferentiation of MG, reprogramming into proliferating MGPCs, and the neuronal differentiation of the progeny of MGPCs. EZH2 (enhancer of zeste 2) is a histone-lysine N-methyltransferase that impacts many cellular processes including proliferation and differentiation (Moritz and Trievel, 2017; Shen and Vakoc, 2015). The canonical functions of EZH2 involve participation in the polycomb repressive complex 2 (PRC2) which suppresses transcription via tri-methylation of H3K27. PRC2 is comprised of not only EZH2, but also regulatory/catalytic subunits EED, SUZ12, RBBP7 and SET. JARID2 and AEBP1 physically associate with PRC2 and facilitate the recruitment of the PRC2 complex to target genes (Kasinath et al., 2021). EZH2 also has non-canonical functions which can include methylation of Stat3 and RORα, transcriptional activation following phosphorylation by JAK3, and methylation-independent promotion of cyclin D,

Notch1 and Wnt-related genes (Moritz and Trievel, 2017; Shen and Vakoc, 2015). EZH2 is known to promote the proliferation of early stage retinal progenitors and differentiation of late-born neurons and glia (Aldiri et al., 2013; Ueno et al., 2017; Zhang et al., 2015). Further, embryonic deletion of *Ezh2* from the retina results in postnatal degeneration of photoreceptors, likely because of failure to suppress embryonic transcription factors (Yan et al., 2016). Some of the gene-repressing actions of EZH2 may be guided by interactions Six3 and Six6, as well as the lcRNA Six3OS (Rapicavoli et al., 2011; Yan et al., 2016), which are prominently expressed by activated MG and MGPCs according to scRNA-seq analysis of cells from mouse and chick retinas (unpublished observations) and immunolabeling in chick retinas (Fischer, 2005). Currently, there is nothing known about the functions of EZH2 or PRC2 in mature MG and during the formation of MGPCs. Accordingly, we investigated how EZH2 influences glial phenotype, de-differentiation MG, proliferation of MGPCs and neuronal differentiation *in vivo*.

**Methods and Materials:**

*Animals:*

The animals approved for use in these experiments was in accordance with the guidelines established by the National Institutes of Health and IACUC at The Ohio State University. Newly hatched P0 wildtype leghorn chicks (*Gallus gallus domesticus*) were obtained from Meyer Hatchery (Polk, Ohio). Post-hatch chicks were maintained in a regular diurnal cycle of 12 hours light, 12 hours dark (lights on at 8:00 AM). Chicks were housed in stainless-steel brooders at 25$^{o}$C and received water and Purina$^{tm}$ chick

starter *ad libitum*.

Mice were kept on a cycle of 12 hours light, 12 hours dark (lights on at 8:00 AM). The use of Ascl1 over-expressing mice (*Glast-CreER:LNL-tTA:tetO-mAscl1-ires-GFP)* was as previously described (Jorstad et al., 2017; Palazzo et al., 2021).

*Intraocular injections:*

Chicks were anesthetized with 2.5% isoflurane mixed with oxygen from a non-rebreathing vaporizer. The technical procedures for intraocular injections were performed as previously described (Fischer et al., 1998). With all injection paradigms, both pharmacological and vehicle treatments were administered to the right and left eye respectively. Compounds were injected in 20 μl sterile saline with 0.05 mg/ml bovine serum albumin added as a carrier. Compounds included: NMDA (38.5nmol or 154 μg/dose; Sigma-Aldrich), FGF2 (250 ng/dose; R&D systems), DZNexp4 (10 μg/dose in DMSO; Tocris), EED226 (10 μg/dose in DMSO; Tocris), UNC1999 (10 μg/dose in DMSO; Tocris), GSK126 (10 μg/dose in DMSO; Tocris), GSK343 (10 μg/dose in DMSO; Tocris), JIB 04 (10 μg/dose in DMSO; Tocris). 5-Ethynyl-2´-deoxyuridine (EdU; 2.3 μg/dose) was intravitreally injected to label the nuclei of proliferating cells. Injection paradigms are included in each figure.

Mice were anesthetized via inhalation of 2.5% isoflurane in oxygen and intraocular injections performed as described previously (Palazzo et al., 2021; Todd et al., 2015; Todd et al., 2019). Right eyes of mice were injected with the experimental compound and the contra-lateral left eyes were injected with a control vehicle. Compounds used in these studies included N-methyl-D-aspartate (NMDA; Sigma; 1.5 ul

at concentration of 100mM in PBS), Trichostatin A (TSA; Sigma; 1 ug/dose in DMSO), and DZNexp4 (1 µg/dose in DMSO; Tocris). Tamoxifen (Sigma; 1.5 mg/100 µl corn oil per dose) was applied as 4 consecutive daily intraperitoneal injections.

*Single Cell RNA and ATAC sequencing of retinas*

Retinas were obtained from adult mice and post-hatch chicks. Isolated retinas were dissociated in a 0.25% papain solution in Hank's balanced salt solution (HBSS), pH = 7.4, for 30 minutes, and suspensions were frequently triturated. The dissociated cells were passed through a sterile 70µm filter to remove large particulate debris. Dissociated cells were assessed for viability (Countess II; Invitrogen) and cell-density diluted to 700 cell/µl. Each single cell cDNA library was prepared for a target of 10,000 cells per sample. The cell suspension and Chromium Single Cell 3' V2 or V3 reagents (10X Genomics) were loaded onto chips to capture individual cells with individual gel beads in emulsion (GEMs) using 10X Chromium Controller. cDNA and library amplification for an optimal signal was 12 and 10 cycles respectively. Sequencing was conducted on Illumina HiSeq2500 (Genomics Resource Core Facility, John's Hopkins University) or HiSeq4000/Novaseq (Novogene) with 2x ≤ 100 bp paired-end reads. Fasta sequence files were de-multiplexed, aligned, and annotated using the chick ENSMBL database (Chick-5.0, Ensembl release 94) and Cell Ranger software. Gene expression was counted using unique molecular identifier bar codes, and gene-cell matrices were constructed. Using Seurat and Signac toolkits, Uniform Manifold Approximation and Projection for Dimension Reduction (UMAP) plots were generated from aggregates of multiple scRNA-seq libraries (Butler et al., 2018; Satija et al., 2015).

Seurat was used to construct violin/scatter plots. Significance of difference in violin/scatter plots was determined using a Wilcoxon Rank Sum test with Bonferroni correction. Monocle was used to construct unbiased pseudo-time trajectories and scatter plotters for MG and MGPCs across pseudotime (Qiu et al., 2017a; Qiu et al., 2017b; Trapnell et al., 2012). SingleCellSignalR was used to assess potential ligand-receptor interactions between cells within scRNA-seq datasets (Cabello-Aguilar et al., 2020). To perform Gene Ontology (GO) enrichment analyses lists of DEGs were uploaded to ShinyGo v0.66 (http://bioinformatics.sdstate.edu/go/) .

Genes that were used to identify different types of retinal cells included the following: (i) Müller glia: *GLUL, VIM, SCL1A3, RLBP1*, (ii) MGPCs: *PCNA, CDK1, TOP2A, ASCL1*, (iii) microglia: *C1QA, C1QB, CCL4, CSF1R, TMEM22*, (iv) ganglion cells: *THY1, POU4F2, RBPMS2, NEFL, NEFM*, (v) amacrine cells: *GAD67, CALB2, TFAP2A*, (vi) horizontal cells: *PROX1, CALB2, NTRK1*, (vii) bipolar cells: *VSX1, OTX2, GRIK1, GABRA1*, (viii) cone photoreceptors: *CALB1, GNAT2, OPN1LW*, and (ix) rod photoreceptors: *RHO, NR2E3, ARR3.* The MG have an over-abundant representation in the chick scRNA-seq databases. This likely resulted from a fortuitous capture-bias and/or tolerance of the MG to the dissociation process.

For scATAC-seq, FASTQ files were processed using CellRanger ATAC 2.1.0, annotated using the chick genome (Gallus_gallus-5.0, Ensembl release 84, assembly GRC6a v105), and then aggregated using CellRanger ATAC aggr to create a common peak set. CellRanger ATAC aggr output was processed and analyzed using Signac (develop version 1.6.0.9015, github.com/timoast/signac) (Stuart et al., 2021) as described elsewhere (https://satijalab.org/signac/articles/mouse_brain_vignette.html).

Annotations were added as an AnnotationHub (Bioconductor.org) object generated from the Ensembl chicken genome (see above). Motif analysis was performed using Signac, the JASPAR 2020 vertebrate database (Fornes et al., 2020), and TFBSTools (Tan and Lenhard, 2016) as described in: https://satijalab.org/signac/articles/motif_vignette.html. Motif scores were generated by analysis of the Signac object using chromVAR (Schep et al., 2017). For Signac and chromVAR motif analysis, the genome used was a FaFile generated using Rsamtools (Bioconductor.org) and the necessary chicken FASTA and index files from Ensembl. For scATAC-seq analysis, including motif enrichment and motif scoring, all reference or annotation genomes were in NCBI/Ensembl format.

*Fixation, sectioning and immunocytochemistry:*

Retinal tissue samples were formaldehyde fixed, sectioned, and labeled via immunohistochemistry as described previously (Fischer et al., 2008a; Fischer et al., 2009c). Antibody dilutions and commercial sources used in this study are described in Table 1. Observed labeling was not due to off-target labeling of secondary antibodies or tissue autofluorescence because sections incubated with secondary antibodies alone were devoid of fluorescence. Patterns of immunolabeling for all antibodies precisely match patterns of mRNA expression in scRNA-libraries of control and damaged retinas, similar previous descriptions (Campbell et al., 2019; Campbell et al., 2021c; Campbell et al., 2021d; Todd et al., 2019). Secondary antibodies utilized include donkey-anti-goat-Alexa488/568, goat-anti-rabbit-Alexa488/568/647, goat-anti-mouse-Alexa488/568/647, goat-anti-rat-Alexa488 (Life Technologies) diluted to 1:1000 in PBS and 0.2% Triton X-100.

*Labeling for EdU:*

For the detection of nuclei that incorporated EdU, immunolabeled sections were fixed in 4% formaldehyde in 0.1M PBS pH 7.4 for 5 minutes at room temperature. Samples were washed for 5 minutes with PBS, permeabilized with 0.5% Triton X-100 in PBS for 1 minute at room temperature and washed twice for 5 minutes in PBS. Sections were incubated for 30 minutes at room temperature in a buffer consisting of 100 mM Tris, 8 mM $CuSO_4$, and 100 mM ascorbic acid in $dH_2O$. The Alexa Fluor 568 Azide (Thermo Fisher Scientific) was added to the buffer at a 1:100 dilution.

*Terminal deoxynucleotidyl transferase dUTP nick end labeling (TUNEL):*

The TUNEL assay was implemented to identify dying cells by imaging fluorescent labeling of double stranded DNA breaks in nuclei. The *In Situ* Cell Death Kit (TMR red; Roche Applied Science) was applied to fixed retinal sections as per the manufacturer's instructions.

*Photography, measurements, cell counts and statistics:*

Microscopy images of retinal sections were captured with the Leica DM5000B microscope with epifluorescence and the Leica DC500 digital camera. High resolution confocal images were obtained with a Leica SP8 available in the Department of Neuroscience Imaging Facility at the Ohio State University. Representative images are modified to optimize color, brightness and contrast using Adobe Photoshop. For quantification of numbers of $EdU^+$ cells, a fixed region of retina was counted and

average numbers of Sox2+/CD45+ and EdU co-labeled cells. The retinal region selected cell counts was standardized between treatment and control groups to reduce variability and improve reproducibility.

Similar to previous reports (Fischer et al., 2009a; Fischer et al., 2009b; Ghai et al., 2009), immunofluorescence was quantified by using Image J (NIH). Identical illumination, microscope, and camera settings were used to obtain images for quantification. Measurement for immunofluorescence were made from single optical confocal sections. Measurements of pS6, pStat3 and pSmad1/5/8 immunofluorescence were made for a fixed, cropped area (25,000 $\mu m^2$) of INL, OPL and ONL. Activation of cell signaling through mTor (pS6), Jak/Stat (pStat3) and BMP/SMAD (pSmad1/5/8) in outer layers of NMDA-damaged retinas is known to manifest exclusively in MG (Todd et al., 2016a; Todd et al., 2017; Zelinka et al., 2016). Measurements were made for regions containing pixels with intensity values of 70 or greater (0 = black and 255 = saturated). The cropped areas contain between 80 and 140 MG or MGPCs; numbers of cells vary depending on treatments that influence the proliferation of MGPCs. The intensity sum was calculated as the total of pixel values for all pixels within threshold regions. GraphPad Prism 6 was used for statistical analyses.

We performed a Levene's test to determine whether data from control and treatment groups had equal variance. For treatment groups where the Levene's test indicated unequal variance, we performed a Mann Whitney U test (Wilcoxon Rank Sum Test). For statistical evaluation of parametric data we performed a two-tailed paired *t*-test to account for intra-individual variability where each biological sample served as its own control (left eye – control; right eye – treated). For multivariate analysis across >2

treatments we performed an ANOVA with the associated Tukey Test to evaluate significant differences between multiple groups.

**Results:**

**Expression of PRC2 components in normal and damaged retinas:**

To assess patterns of expression of the different components of the PRC2 complex we probed previously established scRNA-seq libraries (Campbell et al., 2019; Campbell et al., 2021b; Campbell et al., 2021c; Hoang et al., 2020). scRNA-seq libraries were generated and aggregated for retinal cells obtained from control and NMDA-damaged retinas at different times (24, 48 and 72 hrs) after treatment (Fig. 1a). UMAP plots were generated and clusters of different cells were identified based on well-established patterns of expression (Fig. 1a). For example, resting MG formed a discrete cluster of cells and expressed high levels of *GLUL, RLBP1* and *SLC1A3* (Fig. 1b). After damage, MG downregulated markers of mature glia as they transition into reactive glial cells and into dividing progenitor-like cells, which upregulate *TOP2A, CDK1* and *ESPL1* (Fig. 1b).

The expression of *EZH2* and *EED* was scattered in oligodendrocytes and Non-astrocytic Inner Retinal Glia (NIRGs). NIRG cells are a distinct type of glial cells that has been described in the retinas of birds (Fischer et al., 2010; Rompani and Cepko, 2010) and some types of reptiles (Todd et al., 2016b). In addition, *EZH2* and *EED* were detected in scattered amacrine cells, bipolar cells and cone photoreceptors (Fig. 1c). *SET* was widely expressed across all types of retinal cells (Fig. 1c). Activators of EZH2,

*JARID2* and *AEBP1*, were prominently expressed by inner retinal neurons, including amacrine and bipolar cells (Fig. 1c).

To perform a more detailed analysis we bioinformatically isolated the MG and re-ordered these cells across pseudotime. Pseudotime analysis and violin/scatter plots of MG/MGPCs in different pseudotime states revealed a branched trajectory with resting MG, proliferating MGPCs, and activated MG from 72hr after NMDA-treatment largely confined to different branches and 5 different pseudotime states (Fig. 1d,f). The expression of *EZH2* across pseudotime positively correlates with a transition toward an MGPC-phenotype and upregulation of progenitor markers, such as *CDK1*, and inversely correlates with resting glial phenotypes with significant downregulation of glial markers such as *GLUL* (Fig. 1d-f). By comparison, levels of *EED* and *SET* were significantly increased in pseudotime state 4, corresponding to the largest decrease in activated MG compared to resting MG (Fig. 1d-f). Collectively, these observations suggest that expression levels of *EZH2* and PRC2-components are elevated in MGPCs.

To validate some of the findings from scRNA-seq, we performed immunolabeling for EZH2. We detected no significant immunofluorescence for EZH2 in undamaged retinas (Fig. 1g). By comparison, at 24hrs after NMDA-treatment we observed low levels of EZH2-immunoreactivity in the nuclei of cells near the middle of the INL and nuclei scattered across the IPL (Fig. 1g). At 48 and 72hrs after NMDA-treatments EZH2-immunoreactivity was prevalent in numerous nuclei in the INL and scattered across the IPL (Fig. 1g). Nearly all of the EZH2-positive nuclei in the INL were Sox9-positive MG (Fig. 1h). The EZH2-positive nuclei in the IPL where either Sox9-positive NIRG cells (Fig. 1h) or CD45-positive microglia (Fig. 1i). The patterns of EZH2-immunolabeling

closely match patterns of expression seen in scRNA-seq libraries of NMDA-damaged retinas.

**Inhibition of EZH2 in damaged retinas:**

To test whether EZH2 influences the formation of MGPCs, we applied the inhibitor 3-Deazaneplanocin A hydroclodride (hereafter referred to as DZN) in conjunction with NMDA-treatment. DZN is a 3-deazaadenosine homolog that was first discovered as an inhibitor of S-adenosylhomocysteine hydrolase and is a potent inhibitor of EZH2 (Miranda et al., 2009; Tan et al., 2007). Cellular proliferation is an integral step and read-out of MG becoming progenitor-like cells (Fischer and Bongini, 2010; Fischer and Reh, 2003). We found that inhibition of EZH2 potently suppressed numbers of proliferating MGPCs that accumulated EdU or expressed PCNA, pHisH3 or neurofilament compared to numbers of MGPCs in control retinas (Fig. 2a-d). Similarly, DZN-treatment suppressed the reactivity (upregulation of CD45), accumulation ($DAPI^+/CD45^+$), and proliferation ($EdU^+/CD45^+$) of microglia (Fig. 2e-g). scRNA-seq analyses of microglia indicated that *EZH2, SET, RBBP4, JARID2* and *AEBP1* are significantly upregulated in damaged retinas (Supplemental Fig. 1). DZN treatment had no significant effect upon the NIRG cells (Supplemental Fig. 2a,b) or numbers of $TUNEL^+$ dying cells (Fig. 2h,i) in NMDA-damaged retinas. We found that 3 consecutive daily intraocular injections of DZN alone had no effects upon the reactivity of MG (not shown) or cell death (Supplemental Fig. 2c). Total numbers of $Sox2^+$ MG nuclei were significantly reduced in NMDA-damaged retinas treated with DZN, but this was not significantly different from numbers seen in undamaged, saline-treated retinas

(Supplemental Fig. 2d,e), consistent with the notion that DZN-treatment blocks the proliferation of MGPCs without killing MG. DZN-treatment had no significant effect on the number of neurons produced by MGPCs (data not shown). Collectively, these finding suggest that inhibition of EZH2 in damaged retinas potently suppresses the formation of proliferating MGPCs without destroying Müller glia or influencing neuronal cell death.

**Histone methylation in MG**

We next investigated whether inhibition of EZH2 influenced histone methylation by applying antibodies to Histone H3 K27 trimethyl (H3K27me3). H3K27me3 is associated with transcriptional silencing (Cheung and Lau, 2005; Margueron et al., 2005). Immunofluorescence for H3K27me3 was observed in most, if not all, retinal cells. Compared to levels of H3K27me3 immunofluorescence in the nuclei of resting MG in undamaged retinas, levels of were not significantly different in the nuclei of activated MG in damaged retinas at 48hrs after treatment (not shown). Levels of H3K27me3 were significantly reduced in area, average intensity per nuclei, and intensity sum in MG nuclei treated with DZN (Fig. 3a-d). Levels of H3K27me3 appeared reduced in outer retinal layers following treatment with DZN (Fig. 3a). Indeed, the average level of H3K27me3 per nuclei and intensity sum for the whole retina was significantly reduced in NMDA-damaged retinas treated with DZN (Fig. 3e,f). The DZN-induced decrease in density sum for H3K27me3 remained significant when omitting H3K27me3 immunofluorescence in the nuclei of MG (Fig. 3g).

**Inhibition of EED and JARID2**

To further investigate whether PRC2 activity influences the formation of MGPCs we applied an additional inhibitor to EZH2 and inhibitors to EED and JARID2. UNC1999 inhibits EZH2 with an $IC_{50}$ of ~2nM with 22-fold selectively over EZH1 and >1000-fold selectivity for other histone methyltransferases (Konze et al., 2013). Astemizole was identified as a second generation antihistamine, but has also been reported to interfere with the interactions of EED with EZH2 (Du et al., 2021, 2; Kong et al., 2014). EEDi (EED226) has an $IC_{50}$ between 20-60 nM and competitively acts at the H3K27me3 binding pocket of EED (Qi et al., 2017). Jib04 is a pan-selective Jumonji D (JMJD) histone demethylase inhibitor with $IC_{50}$ between 230-1100 nM (Konze et al., 2013). Similar to the effects seen for DZN, we found that UNC1999 (EZH2 inhibitor), EEDi (EED inhibitor) and Jib04 (JMJD inhibitor) significantly reduced numbers of proliferating MGPCs in damaged retinas (Fig. 4a,b). By contrast, astemizole (putative EED inhibitor), had no effect on the proliferating MGPCs in damaged retinas (Fig. 4a,b). Accordingly, we did not further analyze the effects of astemizole. Numbers of TUNEL-positive cells were not significantly affected by UNC1999, EEDi or Jib04 in NMDA-damaged retinas (Fig. 4c,d). Numbers of proliferating EdU+/CD45+ microglia/macrophage were significantly decreased in damaged retinas treated with UNC1999 or Jib04 (Fig. 4e-g). This is consistent with scRNA-seq data that indicate that *EZH2* and *JARID2* are upregulated in activated microglia (Supplemental Fig.1). By contrast, the proliferation of microglia was significantly increased in damaged retinas treated with EEDi (Fig. 4e-g), despite scRNA-seq data indicating that microglia do not express *EED* in normal or damaged retinas (Supplemental Fig.1). This finding suggests that the increased

proliferation of EEDi-treated microglia may occur via indirect or off-target actions. Collectively, these findings indicate that activity of PRC2 complex and JARID2 are required for the formation of proliferating MGPCs. It must be noted that Jib04 may also be eliciting effects through other JMJD isoforms, including *JMJD1C, JMJD4* and *JMJD6*, with *JMJD1C* and *JMJD4* having dynamic patterns of expression in MG and microglia following NMDA-treatment (Supplemental Fig. 3). Although inhibition of EZH2 or JMJDs suppressed the proliferation of microglia, inhibition of EED had the opposite effect.

**Changes in chromatin access and gene expression following inhibition of EZH2:**

We treated normal and NMDA-damaged retinas treated with vehicle or DZN and harvested retinal cells to generate scATAC-seq and scRNA-seq libraries. Following scATAC-seq UMAP embedding of cells revealed distinct clusters of different types of neurons and glia (Fig. 5a,b). We identified clusters of neurons based of elevated chromatin access for genes known to be expressed by MG (*SOX2, NOTCH1, PAX6*), oligodendrocytes and NIRG cells (*NKX2-2, OLIG2*), amacrine cells (*TFAP2A, PAX6*), horizontal cells (*PAX6*), bipolar cells (*OTX2*, *VSX2*), ganglion cells (*ISL2*), cone photoreceptors (*ISL2*, *CALB1*, *GNAT2*), and rod photoreceptors (*RHO*) (Fig. 5c). DZN- and NMDA-treatments had little effect upon UMAP-clustering of retinal neurons, whereas MG from different treatments were spatially separated (Fig. 5a,b,d), indicating that changes in chromatin access resulting from NMDA-treated or inhibition of EZH2 are primarily manifested in MG, but not other types of retinal cells. Unfortunately, very few MG (94 cells) from NMDA+DZN-treated retinas were captured (Fig. 5a), making statistical analysis impossible.

There were significant changes in genes with differentially accessible regions of chromatin (DARC) when comparing scATAC-seq for MG from saline±DZN and NMDA-treated retinas (Fig. 5e-k). Treatment with DZN or NMDA resulted primarily in increased chromatin access in numerous genes, whereas decreased chromatin access occurred for relatively few genes (Fig. 5e). For example, DZN-treatment increased, while NMDA decreased, chromatin access for immediate early genes, such as *FOS, FOSB* and *EGR1*, and markers of resting glia, such as *CDK1NA, CA2* and *GLUL* (Fig. 5e-h). DZN-treatment of undamaged retinas resulted in changes in chromatin access in genes associated with maintaining glial phenotype that are expressed by resting MG such as *GPR37* and *CDKN1A* (Fig. 5e,h). In addition, DZN-treatment of undamaged retinas resulted in changes in chromatin access for many genes that have been implicated in regulating the formation of MGPCs, including signaling pathways for BMP and TGFβ (*TGIF1, TGFB2, BMPR1A, CHRDL1*) (Todd et al., 2017), (Todd et al., 2016a), MAPK-signaling (*FGF1, SPRY2*) (Fischer et al., 2009a; Fischer et al., 2009b), Notch (*HEY1, HES1, DLL1, NOTCH1*) (Ghai et al., 2010; Hayes et al., 2007), Hedgehog (*GLI2, PTCH2*) (Todd and Fischer, 2015), (Gallina et al., 2014b), retinoic acid (*RARA*) (Todd et al., 2018), mTor (*MTOR)* (Zelinka et al., 2016), and pro-inflammatory signaling (*NFKBIB, S1PR1)* (Fig. 5e-h). MG from NMDA-damaged retinas had increased chromatin access to many different genes including different transcription factors and cell signaling pathways, particularly those associated with TGFβ-signaling (Fig. 5e-g, i). In addition, MG from NMDA-damaged retinas had decreased chromatin access for immediate early genes which are known to be upregulated by activated MG (Fischer et al., 2009a; Fischer et al., 2009b), and genes associated with signaling pathways known

to influence the formation of MGPCs including HBEGF (Todd et al., 2015), gp130/JAK/STAT (*JAK1, IL1RAP*) (Todd et al., 2016a), Notch (*NUMB, MAML2*) (Ghai et al., 2010; Hayes et al., 2007), and midkine/pleotrophin (*ITGB3, SDC4*) (Campbell et al., 2021b) (Fig. 5e,i).

We performed gene ontology (GO) enrichment analyses for genes with significant changes in chromatin access in MG resulting from EZH2-inhibition. In MG treated with DZN in the absence of damage, we observed significant increases in chromatin access for gene modules associated with cell signaling pathways including Hippo, thyroid hormone, HIF-1 and Notch-signaling, as well as gene modules associated with neurogenesis, cell migration and eye development (Fig. 5j). By comparison, we observed significant decreases in chromatin access for gene modules associated with cAMP signaling and cell motility in MG in treated with DZN (Fig. 5j). We observed significant increases in chromatin access for gene modules associated with transcription factor activity/binding, TGFβ-signaling, cellular migration and differentiation in MG in damaged retinas (Fig. 5k). By comparison, we observed significant decreases in chromatin access for gene modules associated with neurogenesis and cellular adhesion/morphogenesis in MG in damaged retinas (Fig. 5k).

We next performed scRNA-seq on normal and damaged retinas treated with EZH2 inhibitor. We aggregated scRNA-seq libraries from retinas treated with saline, saline+DZN, NMDA and NMDA+DZN (Fig. 6a,b). DZN-treatment resulted in distinct clustering of MG from the different treatment groups, whereas the UMAP-ordered retinal neurons from different treatments clustered together (Fig. 6b). Resting MG, activated MG and MGPCs were identified based on distinct patterns of expression of *RLBP1,*

*GLUL, SFRP1* (resting), *TGFB2, MDK, PMP2* (activated), and *TOP2A, PCNA, SPC25, CDK1, CCNB2* (MGPCs) (Fig. 6c-e, g-j). The cluster of resting MG was comprised primarily of MG from saline-treated retinas, whereas DZN-treated MG formed a distinct cluster (Fig. 6g-i). The cluster of MGPCs was comprised almost exclusively of MG from NMDA-treated retinas, whereas activated MG was comprised of cells from retinas treated with DZN-saline, DZN-NMDA and NMDA alone (Fig. 6g-i). The cluster of MGPCs correlated well with Cell-Cycle Scoring for cells in S-phase and G2/M-phase (Fig. 6k). We identified numerous differentially expressed genes (DEGs) that were significantly up- or down-regulated in MG in different treatment groups (Fig. 6f). DZN-treatment of MG in undamaged retinas significantly upregulated genes associated with resting MG, glial transcription factors, and cell signaling pathways known to influence MGPC formation (Fig. 6l), including MAPK- (*FGF9, EGF*) (Fischer et al., 2009a; Fischer et al., 2009b), BMP- (*BMPR2*) (Todd et al., 2017) and Wnt-signaling (*WIF1, SFRP1, SFRP2*) (Gallina et al., 2016). By comparison, DZN-treatment of MG in undamaged retinas downregulated genes associated with cell signaling pathways known to influence MGPC formation (Fig. 6l), including midkine/pleotrophin (*MDK, PTN, SDC4*) (Campbell et al., 2021b), Jak/Stat-signaling (*SOCS3*) (Todd et al., 2016a), Notch-signaling (*MAML2*) (Ghai et al., 2010; Hayes et al., 2007) and MMPs (*TIMP2*) (Campbell et al., 2019). DZN-treatment of MG in NMDA-damaged retinas significantly upregulated transcription factors that convey glial identity, such as *VSX2* and *HES1* (Furukawa et al., 2000; Wall et al., 2009), and genes associated with cell signaling pathways, such as MAPK (*MAPK6, SPRY2*) and Wnt/β-catenin (*CTNNB1*) (Fig. 6m). DZN-treatment of MG in NMDA-damaged retinas significantly downregulated genes

associated with chromatin modifications (including *EZH2* and several HMG's), cell cycle progression, transcription factors, and cell signaling factors, particular those related to TGFβ/BMP-signaling which is known to regulate the formation of MGPCs in the chick retina (Fischer et al., 2004; Todd et al., 2017) (Fig. 6m).

We performed GO enrichment analyses for DEGs in MG resulting from EZH2 inhibition in normal and damaged retinas. In DZN-treated MG in undamaged retinas, we observed upregulated DEGs in gene modules associated with neurogenesis, cell migration, cell cycle and cell signaling, namely PI3K-Akt, sphingolipids and the Hedgehog pathway (Fig. 6n). Downregulated DEGs occupied gene modules associated with ribosome biogenesis (Fig. 6n). In DZN-treated MG in damaged retinas, we observed upregulated DEGs in gene modules associated with neurogenesis, eye development, and cell signaling including Wnt and HIF-1 pathways (Fig. 6o). Downregulated DEGs occupied gene modules associated with glial/neuronal differentiation, cellular proliferation, retinal development, cell migration and PI3K-Akt signaling (Fig. 6o).

We next compared the DEGs from scRNA-seq and genes with DARCs from scATAC-seq in MG in undamaged retinas treated with EZH2 inhibitor. We found 127 genes with increased expression and increased chromatin access (Fig. 7a), and these genes included pro-glial transcription factors (*HES1, ID4, NFIX*) and genes highly expressed by resting glia (*GLUL, GPR37, CSPG5, CDKN1A*). We found 21 genes with increased mRNA levels and decreased chromatin access (Fig. 7a), and these genes included those upregulated in reactive glia (*GFAP, VIM*) and cell signaling pathways known to influence MG (*FSTL1, CHRDL1, FOS, SOCS3, TIMP2*) (Campbell et al.,

2019; Gallina et al., 2016; Todd et al., 2016a). There were only 2 genes with decreased mRNA and decreased chromatin access (Fig. 7a).

We next compared the DEGs from scRNA-seq and DARCs from scATAC-seq in MG in saline vs NMDA-damaged retinas. We found 61 genes with increased expression and increased chromatin access (Fig. 7b), and these genes included a pro-glial transcription factor (*HES1*), and genes associated with cell-signaling (*ILRAP1, PI3KCD, ADCYAP1, INSIG2*) and activated glia (*PMP2, TUBB6*). We found 34 genes with decreased mRNA and decreased chromatin access (Fig. 7b), and these genes included those highly expressed by resting MG (*WIF1, GLUL, CA2*) and immediate early genes (*FOS, EGR1*). There were only 2 genes with increased mRNA and decreased chromatin access (Fig. 7b). We were not able to identify genes from scRNA-seq and scATAC-seq in NMDA-damaged retinas treated with EZH2-inhibitor because too few MG were captured in the scATAC libraries.

We next identified transcription factor DNA-binding motifs with differential chromatin access in promoter regions in MG. MG were identified based on significant access to motifs such as *SOX9* (Fig. 7c), *RAX, MSX1* and *VSX2* (not shown). Activated and resting MG were distinguished based of enriched access for motifs for transcriptional effectors of different cell signaling pathways such as *FOS::JUN*, *SMAD2::SMAD3* and *STAT3* (Fig. 7e-g). In addition, we identified significant differences in enriched access to motifs related to NFkB (*NFKB2, RELA*), Hedgehog (*GLI2*), retinoic acid (*RARA*), glucocorticoid (*NR3C2*) and Hippo-signaling pathways (*TEAD1*), which are known to influence the formation of MGPCs (Gallina et al., 2014b; Palazzo et al., 2020; Palazzo et al., 2022; Rueda et al., 2019; Todd and Fischer, 2015; Todd et al.,

2018; Young et al., 2000). We next analyzed levels of mRNA (scRNA-seq), chromatin access (scATAC-seq) and enriched motif access in MG for transcription factors that are known to be important for retinal development and the formation of MGPCs. We observed consistent increases across levels of mRNA, chromatin access and motif enrichment in DZN-treated MG for *NFIA/C/X*, *SOX2/8/9*, *PAX6, VSX2* and *RAX* (Fig. 7i-k). By comparison, we observed consistent increases across levels of mRNA, chromatin access and motif enrichment in NMDA-treated MG for *HES1, HEY1, PAX2, ATF3* and *KLF6* (Fig. 7i-k).

**Implied Ligand-Receptor interactions among MG and microglia:**

We next isolated MG and microglia, re-embedded these cells in UMAP plots and probed for cell signaling networks and putative ligand-receptor interactions using SingleCellSignalR (Cabello-Aguilar et al., 2020). We focused our analyses on MG and microglia because there is significant evidence to indicate autocrine and paracrine signaling among these cells in the context of glial reactivity and the formation of MGPCs (Fischer et al., 2014b; Wan et al., 2012b; White et al., 2017; Zelinka et al., 2012). UMAP plots revealed distinct clusters of resting MG (*GLUL, GPR37, RLBP1*) from saline and saline-DZN libraries, activated MG (*MDK, HBEGF, TGFB2*), MGPCs (*TOP2A. SPC25, CDK1*) and a cluster of microglia (*C1QA, SPI1, CSF1R*) (Figs. 8a-f). Numbers of LR-interactions (significant expression of ligand and receptor) between cell types in the different treatment groups varied from 124 to 292 (Fig. 8g). We identified the 40 most significant paracrine LR-interactions for MG to microglia and microglia to MG for each treatment group (Figs. 8h-k). We next identified paracrine LR-interactions

between glia unique to saline vs saline+DZN treatment groups (Figs. 8l,n). In the saline-treatment group, we found 41 unique paracrine LR-interactions including midkine-, FGF-, TGFβ- and activin-signaling. By comparison, saline+DZN-treatment resulted in 59 unique paracrine LR-interactions between glia such as EGF-, HBEGF-, IGF- and Notch-signaling. In the NMDA-treatment groups (Fig. 8m), we found 30 unique paracrine LR-interactions including FGF- and laminin/integrin-signaling. By comparison, NMDA+DZN-treatment resulted in 29 unique paracrine LR-interactions between glia such as EGF-, HBEGF-, BDNF- vitronectin/integrin- and plasminogen activator urokinase (*PLAU*) -signaling. Many of the above-mentioned pathways have been implicated in the formation of MGPCs in the chick retina including HB-EGF, IGF/FGF/MAPK- , Wnt/-β catenin-, Notch-, TGFβ/Smad- and midkine-signaling (Campbell et al., 2021b; Fischer et al., 2009a; Gallina et al., 2016; Ghai et al., 2010; Hayes et al., 2007; Todd et al., 2015; Todd et al., 2017; Zelinka et al., 2016).

We next identified MG-specific autocrine LR-interactions in saline ± DZN and NMDA ± DZN treatment groups (Figs. 8n,o). Unique to the saline-treatment group for autocrine MG, we found 49 unique LR-interactions including midkine-, Wnt-, FGF- and activin-signaling. By comparison, saline+DZN-treatment resulted in 27 unique autocrine MG LR-interactions such as EGF-, IGF- and GDF/BMPR2-signaling. In the NMDA-treatment groups (Fig. 8o), we found 17 unique autocrine MG LR-interactions including TGFβ- and laminin/integrin-signaling. By comparison, NMDA+DZN-treatment resulted in 42 unique autocrine MG LR-interactions between glia such as FGF-, Notch-, Midkine- , Wnt-, BDNF-, Hepatocyte Growth Factor (HGF) /integrin- and fibronectin (*FN1*) /integrin-signaling. Many of the above-mentioned pathways have been implicated in the

formation of MGPCs in the chick retina including HB-EGF, IGF/FGF/MAPK- , Wnt/β -catenin-, Notch-, BMP/Smad- and midkine-signaling (Campbell et al., 2021b; Fischer et al., 2009a; Gallina et al., 2016; Ghai et al., 2010; Hayes et al., 2007; Todd et al., 2015; Todd et al., 2017; Zelinka et al., 2016).

**Inhibition of EZH2 suppresses mTor signaling in MG in damaged retinas:**

We next investigated whether inhibition of EZH2 influenced cell signaling pathways that promote the formation of MGPCs. cFos, pS6 (mTor-signaling), pStat3 (Jak/Stat-signaling) and pSmad1/5/8 (BMP/Smad-signaling) are known to be rapidly upregulated in MG after NMDA-treatment and activation and promote the formation of proliferating MGPCs (Fischer et al., 2009a; Todd et al., 2016a; Todd et al., 2017; Zelinka et al., 2016). Thus, we applied NMDA ± DZN at P6, vehicle or DZN at P7, and harvested retinas 4hrs after the last injection. At this early time point there was no significant difference in numbers of dying cells with DZN-treatment (Fig. 9a,b), similar to findings at 72hrs after NMDA (Fig. 2h,i). Inhibition of EZH2 had no effect upon damaged-induced increases in cFos, pStat3 or pSmad1/5/8 in MG in damaged retinas (Fig. 9a,c,e,f). By comparison, we found that inhibition of EZH2 resulted in a significant decrease in levels of pS6 in MG in damaged retinas (Fig. 9a,d).

**Inhibition of EZH2 in undamaged retinas and CMZ proliferation**:

To test whether PRC2 was involved in the formation of MGPCs in the absence of retinal damage we used a growth factor-treatment paradigm. Three consecutive daily intraocular injections of insulin and FGF2 are known to be sufficient to induce the

formation of proliferating MGPCs in the absence of damage (Fischer et al., 2002b; Fischer et al., 2014b). We found that components of PRC2 were increased in MG treated with insulin+FGF2, although not as much when compared to levels seen in MG from NMDA-damaged retinas (Supplement Fig.4). Immunolabeling of retinas treated with insulin+FGF2 indicated increased EZH2-immunoreactivity in the nuclei of MG, and this labeling was absent when EZH2 was inhibited by DZN (Fig. 10a). There was a significant decrease in the number of EdU/Sox2-positive nuclei (proliferating MGPCs) in insulin+FGF2-treated retinas where EZH2 was inhibited (Fig. 10b,c). Consistent with these findings, there was a significant decrease in the number of pHisH3/Sox2/neurofilament-positive cells in insulin+FGF2-treated retinas where EZH2 was inhibited (Fig. 10d,e). In central regions of the retina, insulin+FGF2 stimulated the migration of MG nuclei away from the middle of the INL without EdU incorporation (Fig. 10f,g). The migration of nuclei is correlated with the proliferation of MGPCs (Fischer and Reh, 2001), but migration can occur without re-entry into the cell cycle (Fischer et al., 2014b; Todd and Fischer, 2015). Treatment with insulin+FGF2+DZN inhibited the migration of MG nuclei away from the middle of the INL (Fig. 10f,g). The proliferation and reactivity of microglia was unaffected by DZN in insulin+FGF2-treated retinas (not shown). Treatment with insulin and FGF2 is known to stimulate MG to rapidly and transiently upregulate cFos, pSmad1/5/8, pS6 and pStat3 (Fischer et al., 2009c; Todd et al., 2016a; Todd et al., 2017; Zelinka et al., 2016). Inhibition of EZH2 had no effects upon patterns of immunofluorescence for cFos, pStat3 or pS6 (Fig. 10h and not shown), whereas immunofluorescence of pSmad1/5/8 was sustained and elevated in the nuclei of MG (Fig. 10h).

We next investigated whether the proliferation of progenitors in the circumferential marginal zone (CMZ) was influenced by inhibition of EZH2. CMZ progenitors are found at the peripheral edge of the post-hatch chick retina and normally proliferate at relatively low levels, but can be stimulated to proliferate at elevated levels in response to insulin/FGF2 or IGF1 (Fischer and Reh, 2000; Fischer et al., 2002a; Fischer et al., 2008b). We found that application of DZN significantly suppressed the proliferation of CMZ progenitors that is stimulated by insulin+FGF2 (Fig. 10i-k). This finding suggests that EZH2 activity is required for the proliferation of CMZ progenitors, retinal progenitors that are distinctly different from MGPCs.

**PRC2 in the mouse retina**

We probed scRNA-seq libraries from normal and NMDA-damaged mouse retinas, as described previously (Campbell et al., 2021b; Hoang et al., 2020; Todd et al., 2019). UMAP ordering of cells reveal distinct clusters of different types of retinal cells, with only the MG distinctly clustered according to time after NMDA-treatment (Figs. 11a-c). UMAP heatmap plots revealed relatively wide-spread expression of PRC2-related genes, including *Ezh2, Eed, Set, Suz12, Jarid2* and *Aebp2*, in different types of retinal neurons and glia (Figs. 11d-f). Isolation, re-normalize and re-embedding of MG revealed distinct clusters related to the different times after NMDA-treatment (Fig. 11g). The largest differences in gene expression occurring at 3 and 6 hrs after NMDA-treatment (++activated and +activated clusters) (Fig. 11g), which included downregulation of resting glial markers such as *Glul*, and upregulation of activated glial markers such as *Vim* and *Nes* (Fig. 11g). Unlike patterns of expression seen in MG in NMDA-damaged

chick retinas, MG in damaged mouse retinas downregulated levels of *Ezh2, Jarid2, Set* and *Aebp2* downregulated in activated glia at different times after treatment (Fig. 11h).

MG in the adult mouse retina can be reprogrammed to generate neuron-like cells by forced expression of Ascl1 combined with NMDA-induced neuronal damage and HDAC inhibitor to increase chromatin access (Jorstad et al., 2017). We hypothesized that inhibition of EZH2 may influence neurogenic reprogramming in the mouse retina. To test this hypothesis we applied EZH2 inhibitor (DZN) to the retinas of *Glast-CreER:LNL-tTA:tetO-mAscl1-ires-GFP* mice (Jorstad et al., 2017). To induce neuron regeneration from MG treatment with NMDA, neuronal damage and HDAC inhibitor trichostatin A (TSA) are required (Jorstad et al., 2017). Similar to EZH2 inhibitor, HDAC inhibitor is expected to increase chromatin access. Thus, we replaced TSA with DZN in the treatment paradigm. We tested whether inhibition of EZH2 influenced the formation of neurons derived from *Ascl1*-overexpressing MG. *Ascl1* expression in MG was activated by IP delivery of 4 consecutive daily doses of tamoxifen in adult mice (P80-P90). This was followed by intravitreal injection of NMDA or NMDA+DZN on D8 and injection of vehicle or DZN on D10 (Fig. 11i). Eyes were harvested and retinas were processed for immunolabeling 2 weeks after the final injection. Inhibition of *EZH2* in Ascl1-overexpressing MG resulted in no significant change in the de-differentiation of Sox2+ MG (Figs. 11i,k ), or differentiation of Otx2+ neuron-like cells (Figs. 11j,l).

**Discussion:**

We find that components of the PRC2 complex and EZH2-activators *JARID2* and *AEBP1* are dynamically expressed by MG in damaged retinas. Dynamic changes of

mRNA levels are strongly correlated with changes in protein levels and function (Liu et al., 2016). In the chick retina MG upregulated *EZH2* and PRC2-related genes during transition into MGPCs. By contrast, PRC2-related genes were not widely expressed and were downregulated by MG in damaged mouse retinas. Our findings indicate that inhibition of EZH2, EED or JARID2 potently suppress the formation of proliferating MGPCs in the chick retina (Fig. 12). By comparison, inhibition of EZH2 had no effect upon the differentiation of neuron-like cells from Ascl1-over expressing MG in damaged mouse retinas. In the chick, inhibition of EZH2 had significant effects upon gene expression and chromatin access in MG and microglia (Fig. 12). Many changes in expression and access are associated with modules of genes that influence retinal development, neuronal differentiation and cell signaling pathways that are known to influence the formation of proliferating MGPCs. The lack of effects of astemizole on glial cells in the retina likely reflects a lack of specificity. Astemizole is a second generation anti-histamine, but has also been shown to interfere with the interaction of EED with EZH2 (Du et al., 2021; Kong et al., 2014). In summary, the effects of EZH2, EED and JMJ inhibitors are consistent with the notion that the activity of PRC2 is required for the formation of proliferating MGPCs in the chick retina.

**NMDA-induced retinal damage influences chromatin accessibility in MG**

For scATAC-seq libraries, UMAP ordering of cells from control and damaged retinas indicated that MG, unlike other types of retinal cells, had significant differences in chromatin access represented by spatial separation of MG from different treatments. We identified more than 480 genes with differential chromatin access in MG from

NMDA-damaged retinas. These genes included decreased access to many different immediate early genes and genes associated with morphogenesis and neurogenesis, and increased access to genes associated with cell signaling pathways, such as TGFβ, gp130/Jak/Stat and Notch, which are known to influence glial reactivity and formation of MGPCs (Ghai et al., 2010; Todd et al., 2016a; Todd et al., 2017). Changes in chromatin access in glial cells have been well-described during development. For example, the maturation of astrocytes involves extensive changes in chromatin access (Lattke et al., 2021). Similarly, developmental differences in gene expression and chromatin access have been identified and compared across retinal progenitors and MG, and prevalent changes in chromatin access demonstrated for neurogenic genes (VandenBosch et al., 2020).

**Genes affected by EZH2-inhibition**

We observed a modest correlation of genes with increased/decreased chromatin access and increased/decreased expression levels. There were few genes with increased chromatin access and downregulated gene expression. It is possible that heterogeneity of cells within UMAP-clustered MG accounts for diminished correlation between genes with chromatin access and expression levels. A combined multi-omic approach may resolve this possibility wherein individual cells receive unique DNA barcodes and unique molecular identifiers to measure both chromatin access (ATAC-seq) and gene expression (RNA-seq). By comparison, we observed a strong correlation between chromatin access, mRNA levels, and motif access in MG for transcription factors related to glial identity and retinal development. Similarly, a recent stud*y*

identified genomic regions important to corticogenesis by assessing the activity of gene-regulatory elements by mapping, at single-cell resolution, gene expression and chromatin access (Trevino et al., 2021). Networks of gene regulation, including expression programs of glial lineages, were strongly correlated between gene-regulatory elements and expression levels for key transcription factors (Trevino et al., 2021).

**EZH2 inhibition and proliferation of progenitors**

Inhibitors to EZH2, EED and JMJs potently suppressed the formation of proliferating MGPCs. EZH2 inhibition also suppressed the formation of MGPCs in retinas treated with insulin and FGF2 in the absence of neuronal damage, and suppressed the proliferation of stimulated CMZ progenitors at the far peripheral edge of the retina. Collectively, these findings suggest that the activity of EZH2 and PRC2 are required for the proliferation of retinal progenitor cells. Consistent with labeling for proliferation markers in tissue sections, EZH2 inhibition significantly downregulated many proliferation-related genes in MG in damaged retinas. However, inhibition of EZH2 did not significantly influence chromatin access to proliferation-related genes. These observations suggest the changes in chromatin access and gene expression caused by inhibiting EZH2/PRC2 act upon genes that are upstream of regulating re-entry into the cell cycle. However, it is possible that inhibition of the non-canonical actions of EZH2 impact the formation of MGPCs. EZH2 has non-canonical functions including methylation of Stat3 and RORα, transcriptional activation following phosphorylation by JAK3, and methylation-independent promotion of cyclin D, Notch1

and Wnt-related genes (Moritz and Trievel, 2017; Shen and Vakoc, 2015). Jak/Stat-, Notch- and Wnt-signaling are known to promote the formation of proliferating MGPCs in the chick retina (Gallina et al., 2016; Ghai et al., 2010; Hayes et al., 2007; Todd et al., 2016a). Consistent with our findings regarding the influence of EZH2 activity on the proliferation of MGPCs and CMZ-progenitors, EZH2-activity promotes the proliferation of early-stage progenitors and differentiation of late-born neurons and glia in the developing retina (Aldiri et al., 2013; Ueno et al., 2017; Zhang et al., 2015). In the mouse retina, some of the gene-repressing actions of EZH2 may be guided by interactions Six3 and Six6 (Rapicavoli et al., 2011). Consistent with these findings, *SIX3* and *SIX6* are prominently expressed by resting MG, upregulated in MG in response to EZH2 inhibitor, and downregulated by activated MG and MGPCs in damaged retinas, and this is coordinated with changes in chromatin access.

**EZH2 and cell signaling in MG**

Inhibition of EZH2 in undamaged retinas stimulated MG to upregulate genes associated with resting MG, pro-glial transcription factors, and cell signaling pathways known to stimulate and suppress MGPC formation. For example, treatment with EZH2 inhibitor upregulated some of the most highly expressed genes in resting MG including *GLUL, RLBP1, CSPG5* and *GPR37*. In addition, treatment with EZH2 inhibitor upregulated transcription factors, such as *ID4* and *NFIA/C/X*, which are known to promote glial differentiation and maintain glial identity (Clark et al., 2019; Deneen et al., 2006) and transcription factors, such as *SIX3* and *SIX6*, which are known to maintain retinal progenitor cells (Diacou et al., 2018). Further, we observed upregulation of Wnt

suppressors such as *WIF1*, *SFRP1* and *SFRP2,* which are expected to suppress MGPC formation, since Wnt-signaling promotes the proliferation of MGPCs (Gallina et al., 2016) and upregulation of MAPK-associated genes are expected to increase MGPC formation (Fischer et al., 2009a; Fischer et al., 2009b). However, the EZH2 inhibitor did not induce the formation of MGPCs in undamaged retinas, suggesting that the upregulation of pro-glial networks supersedes any upregulation of pro-MGPC cell signaling pathways. Collectively, these findings indicate inhibition of EZH2 in undamaged retinas predominantly activates networks that promote glial phenotype and reprogramming into progenitors.

Inhibition of EZH2 in undamaged retinas caused MG to downregulate genes associated with cell signaling pathways expected to promote MGPC formation, including midkine/pleotrophin (*MDK, PTN, SDC4*) (Campbell et al., 2021b), Jak/Stat-signaling (*SOCS3*) (Todd et al., 2016a), Notch-signaling (*MAML2*) (Ghai et al., 2010; Hayes et al., 2007) and MMPs (*TIMP2*) (Campbell et al., 2019). DZN-treatment of MG in NMDA-damaged retinas resulted in upregulation transcription factors such as *HES1* and downregulation of *ID3,* which are known to promote glial development and identity, and downregulation of TFs such as *ID3* (Furukawa et al., 2000; Wall et al., 2009). By comparison, *MSX1* is downregulated in MG with EZH2 inhibition; MSX1 is expected to promote the phenotype of peripheral retinal progenitors (Belanger et al., 2017). Nevertheless, EZH2 inhibition in undamaged retinas did not result in the formation of MGPCs. Although inhibition of EZH2 stimulated MG in undamaged retinas to upregulate gene modules associated with neurogenesis and pro-proliferation, the context is changed in damaged retinas and some of these effects are absent or opposite. For

example, gene modules associated with cell migration, PI3K-Akt-signaling and cell cycle are upregulated in MG in undamaged retinas whereas these gene modules are downregulated in MG in damaged retinas. We found that DZN treatment influenced gene expression and chromatin accessibility in undamaged retinas, wherein levels of EZH2 were relatively low. These effects of EZH2 inhibitor on resulting MG may result from: (i) inhibition of low levels of EZH2 in MG, (ii) inhibition of the non-canonical functions of EZH2, or (iii) off-target effects. DZN is known to inhibit S-adenosylhomocysteine hydrolase (AHCY) [recently reviewed in (Vizán et al., 2021)]. *AHCY* is widely expressed by retinal neurons and MG; levels of expression are high in resting glia, downregulated in activated glia, and unchanged in retinal neurons following damage (not shown). AHCY regulates the concentration of intracellular S-adenosylhomocysteine which is important for transmethylation reactions (Vizán et al., 2021). Thus, some of the observed effects of DZN may have resulted from actions at AHCY. For example, decreased levels of H3K27me3 in DZN-treated retinas may have resulted from inhibition of AHCY and depletion of S-adenosylhomocysteine which secondarily would suppress transmethylation reactions including methylation of Histone H3.

Inhibition of EZH2 in damaged retinas resulted in increased autocrine LR-interactions in MG for pathways involving SFRP1 (to inhibit Wnt) and Jagged-Notch. Wnt-signaling stimulates the proliferation of MGPCs in zebrafish (Meyers et al., 2012; Ramachandran et al., 2011b), chick (Gallina et al., 2016) and mouse retinas (Osakada et al., 2007; Yao et al., 2016). The relationship of Notch-signaling to the formation of proliferating MGCPs is more complicated and appears to require dynamic regulation. In

short, evidence suggests that Notch-signaling maintains glial phenotype in resting glia, downregulation is required early for de-differentiation, upregulation is required for proliferation of MGPCs and downregulation is required for neuronal differentiation (Campbell et al., 2021a; Campbell et al., 2022b; Ghai et al., 2010; Hayes et al., 2007; Lee et al., 2020; Sahu et al., 2021). Many of the autocrine LR-interactions induced by EZH2 inhibitor in damaged retina, including those related FGFR1, Notch and midkine-signaling, are expected to promote the formation of MGPCs (Campbell et al., 2021b; Fischer et al., 2009a; Ghai et al., 2010). Similarly, we observed upregulation of many genes associated with different cell signaling pathways, such as *SPRY2* and *IGFBP5,* which are expected to suppress the formation of MGPCs by inhibiting MAPK signaling (Fischer et al., 2009a; Fischer et al., 2009b). By comparison, we observed downregulation of *BMP4* and *SMAD5* which is consistent with suppressed formation of MGPCs (Todd et al., 2017). This is contrary to expectations since EZH2 potently suppressed the formation of MGPCs. In summary, DZN-induced changes in genes and modules associated with cell signaling pathways known to influence the formation of MGPCs are not entirely consistent with suppressing the formation of MGCPs.

Although changes in gene expression and putative LR-interactions implicated changes in cell signaling pathways, we did not observe decreased activation of cFos, Jak/Stat- or BMP/Smad-signaling in MG from damaged retinas treated with EZH2 inhibitor. However, we did observed a significant decrease in mTor-signaling in MG in damaged retinas treated with EZH2 inhibitor; wherein mTor-signaling is known to be required for the formation of MGPCs in damaged chick retinas (Zelinka et al., 2016). By comparison, inhibition of Fatty acid-binding proteins (FABPs) or Fatty acid synthase

(FASN) potently reduces levels of pS6, pStat3 and pSmad1/5/8 in MG in damaged retinas (Campbell et al., 2022a). Collectively, these findings suggest the EZH2 inhibition predominantly acts by modulating chromatin access, changes in expression of pro-glial transcription factors, and access to TF motifs, rather than influencing cell signaling, while potently suppressing cell division and the formation of MGPCs.

**Inhibition of EZH2 in damaged mouse retinas**

Inhibition of EZH2 in the developing mouse retina suppresses the formation of MG (Iida et al., 2015; Zhang et al., 2015, 2). Factors and cell signaling pathways that influence the development of MG also influence the formation of MGPCs in mature damaged retinas. These factors and pathways include Notch/Hes- (Ghai et al., 2010; Hayes et al., 2007), glucocorticoid- (Gallina et al., 2014b), Wnt/β-catenin (Gallina et al., 2016; Osakada et al., 2007; Ramachandran et al., 2011b), FGF/MAPK (Fischer et al., 2009a; Fischer et al., 2009b), and BMP/Smad (Todd et al., 2017). However, EZH2 was not expressed by resting or activated MG in the mouse retina. Thus, it is not surprising the EZH2 inhibitor had no effect on the formation of neuron-like cells from Ascl1-overexpressing MG in damaged mouse retinas.

**Conclusions**:

Our findings indicate that activation of PRC2 is necessary for the formation of proliferating MGPCs and the proliferation of CMZ retinal progenitors in the chick retina. Inhibition of EZH2 significantly modulated signaling networks through changes in chromatin access and gene expression, and most of these changes were manifested in

MG and microglia. Activation of cell signaling pathways known to promote the formation of MGPCs were largely unaffected by EZH2 inhibition, with the exception of signaling through mTor. Collectively, our findings indicate that inhibition of EZH2 results in changes in DEGs and DACRs for genes that are known to promote or inhibit gliogenesis and MGPC formation, and the genes that inhibit MGPC formation supersede those that promote this process in chick retinas. By comparison, PRC2-related genes are downregulated in MG in damaged mouse retinas and inhibition of EZH2 had no effect upon the formation of neuron-like cells from Ascl1-overexpressing MG. We propose that the activity of EZH2 and PRC2 may be among the key differences in avian and mammalian MG that is required for chromatin remodeling that promotes the formation of MGPCs and retinal regeneration.

**Acknowledgements:** We thank Drs. Tim Stuart and Jared Tangeman for providing assistance with establishing appropriate reference genome libraries for scATAC-seq libraries.

**Author contributions:** WAC and HME – experimental design, execution of experiments, collection of data, data analysis, construction of figures, bioinformatics, preparation of RNA-seq and ATAC-seq and writing the manuscript. DT, ECH, LEK, LV and DA – execution of experiments and collection of data. AJF – experimental design, data analysis, bioinformatics, construction of figures and writing the manuscript.

**Data availability**:

Gene-Cell matrices for scRNA-seq data for libraries from saline and NMDA-treated retinas are available through GitHub: https://github.com/jiewwwang/Singlecell-retinal-regeneration

Gene-Cell matrices for scRNA-seq data for libraries for NMDA-treated retinas and DZNexp4-treated retinas are available through GitHub: https://github.com/fischerlab3140/

Gene-Cell matrices for scATAC-seq data are available through GitHub: https://github.com/fischerlab3140/

scRNA-Seq data for chick retinas treated with NMDA or insulin and FGF2 can be queried at: https://proteinpaint.stjude.org/F/2019.retina.scRNA.html.

**References:**

**Aldiri, I., Moore, K. B., Hutcheson, D. A., Zhang, J. and Vetter, M. L.** (2013). Polycomb repressive complex PRC2 regulates Xenopus retina development downstream of Wnt/beta-catenin signaling. *Development* **140**, 2867–78.

**Belanger, M. C., Robert, B. and Cayouette, M.** (2017). Msx1-Positive Progenitors in the Retinal Ciliary Margin Give Rise to Both Neural and Non-neural Progenies in Mammals. *Dev Cell* **40**, 137–150.

**Bernardos, R. L., Barthel, L. K., Meyers, J. R. and Raymond, P. A.** (2007). Late-stage neuronal progenitors in the retina are radial Muller glia that function as retinal stem cells. *J Neurosci* **27**, 7028–40.

**Bringmann, A., Pannicke, T., Grosche, J., Francke, M., Wiedemann, P., Skatchkov, S. N., Osborne, N. N. and Reichenbach, A.** (2006). Muller cells in the healthy and diseased retina. *Prog Retin Eye Res* **25**, 397–424.

**Bringmann, A., Iandiev, I., Pannicke, T., Wurm, A., Hollborn, M., Wiedemann, P., Osborne, N. N. and Reichenbach, A.** (2009). Cellular signaling and factors involved in Müller cell gliosis: neuroprotective and detrimental effects. *Prog. Retin. Eye Res.* **28**, 423–451.

**Butler, A., Hoffman, P., Smibert, P., Papalexi, E. and Satija, R.** (2018). Integrating single-cell transcriptomic data across different conditions, technologies, and species. *Nat. Biotechnol.* **36**, 411–420.

**Cabello-Aguilar, S., Alame, M., Kon-Sun-Tack, F., Fau, C., Lacroix, M. and Colinge, J.** (2020). SingleCellSignalR: inference of intercellular networks from single-cell transcriptomics. *Nucleic Acids Res.* **48**, e55.

**Campbell, W. A., Deshmukh, A., Blum, S., Todd, L., Mendonca, N., Weist, J., Zent, J., Hoang, T. V., Blackshaw, S., Leight, J., et al.** (2019). Matrix-metalloproteinase expression and gelatinase activity in the avian retina and their influence on Müller glia proliferation. *Exp. Neurol.* **320**, 112984.

**Campbell, L. J., Hobgood, J. S., Jia, M., Boyd, P., Hipp, R. I. and Hyde, D. R.** (2021a). Notch3 and DeltaB maintain Müller glia quiescence and act as negative regulators of regeneration in the light-damaged zebrafish retina. *Glia* **69**, 546–566.

**Campbell, W. A., Fritsch-Kelleher, A., Palazzo, I., Hoang, T., Blackshaw, S. and Fischer, A. J.** (2021b). Midkine is neuroprotective and influences glial reactivity and the formation of Müller glia-derived progenitor cells in chick and mouse retinas. *Glia* **69**, 1515–1539.

**Campbell, W. A., Blum, S., Reske, A., Hoang, T., Blackshaw, S. and Fischer, A. J.** (2021c). Cannabinoid signaling promotes the de-differentiation and proliferation of Müller glia-derived progenitor cells. *Glia*.

**Campbell, W. A., Tangeman, A., El-Hodiri, H. M., Hawthorn, E. C., Hathoot, M., Hoang, T., Blackshaw, S. and Fischer, A. J.** (2021d). *Fatty acid-binding proteins and fatty acid synthase influence glial reactivity and promote the formation of Müller glia-derived progenitor cells in the avian retina*.

**Campbell, W. A., Tangeman, A., El-Hodiri, H. M., Hawthorn, E. C., Hathoot, M., Blum, S., Hoang, T., Blackshaw, S. and Fischer, A. J.** (2022a). Fatty acid-binding proteins and fatty acid synthase influence glial reactivity and promote the formation of Müller glia-derived progenitor cells in the chick retina. *Dev. Camb. Engl.* dev.200127.

**Campbell, L. J., Levendusky, J. L., Steines, S. A. and Hyde, D. R.** (2022b). Retinal regeneration requires dynamic Notch signaling. *Neural Regen. Res.* **17**, 1199–1209.

**Cheung, P. and Lau, P.** (2005). Epigenetic regulation by histone methylation and histone variants. *Mol. Endocrinol. Baltim. Md* **19**, 563–573.

**Clark, B. S., Stein-O'Brien, G. L., Shiau, F., Cannon, G. H., Davis-Marcisak, E., Sherman, T., Santiago, C. P., Hoang, T. V., Rajaii, F., James-Esposito, R. E., et al.** (2019). Single-Cell RNA-Seq Analysis of Retinal Development Identifies NFI Factors as Regulating Mitotic Exit and Late-Born Cell Specification. *Neuron* **102**, 1111-1126.e5.

**Conner, C., Ackerman, K. M., Lahne, M., Hobgood, J. S. and Hyde, D. R.** (2014). Repressing Notch Signaling and Expressing TNFalpha Are Sufficient to Mimic Retinal Regeneration by Inducing Muller Glial Proliferation to Generate Committed Progenitor Cells. *J Neurosci* **34**, 14403–19.

**Deneen, B., Ho, R., Lukaszewicz, A., Hochstim, C. J., Gronostajski, R. M. and Anderson, D. J.** (2006). The transcription factor NFIA controls the onset of gliogenesis in the developing spinal cord. *Neuron* **52**, 953–968.

**Diacou, R., Zhao, Y., Zheng, D., Cvekl, A. and Liu, W.** (2018). Six3 and Six6 Are Jointly Required for the Maintenance of Multipotent Retinal Progenitors through Both Positive and Negative Regulation. *Cell Rep.* **25**, 2510-2523.e4.

**Du, D., Xu, D., Zhu, L., Stazi, G., Zwergel, C., Liu, Y., Luo, Z., Li, Y., Zhang, Y., Zhu, K., et al.** (2021). Structure-Guided Development of Small-Molecule PRC2 Inhibitors Targeting EZH2-EED Interaction. *J. Med. Chem.* **64**, 8194–8207.

**Fausett, B. V., Gumerson, J. D. and Goldman, D.** (2008). The proneural basic helix-loop-helix gene ascl1a is required for retina regeneration. *J Neurosci* **28**, 1109–17.

**Fischer, A. J.** (2005). Neural regeneration in the chick retina. *Prog. Retin. Eye Res.* **24**, 161–182.

**Fischer, A. J. and Bongini, R.** (2010). Turning Müller glia into neural progenitors in the retina. *Mol. Neurobiol.* **42**, 199–209.

**Fischer, A. J. and Reh, T. A.** (2000). Identification of a proliferating marginal zone of retinal progenitors in postnatal chickens. *Dev. Biol.* **220**, 197–210.

**Fischer, A. J. and Reh, T. A.** (2001). Muller glia are a potential source of neural regeneration in the postnatal chicken retina. *Nat Neurosci* **4**, 247–52.

**Fischer, A. J. and Reh, T. A.** (2003). Potential of Müller glia to become neurogenic retinal progenitor cells. *Glia* **43**, 70–76.

**Fischer, A. J., Seltner, R. L. P., Poon, J. and Stell, W. K.** (1998). Immunocytochemical characterization of quisqualic acid- and N-methyl-D-aspartate-induced excitotoxicity in the retina of chicks. *J. Comp. Neurol.* **393**, 1–15.

**Fischer, A. J., Dierks, B. D. and Reh, T. A.** (2002a). Exogenous growth factors induce the production of ganglion cells at the retinal margin. *Dev. Camb. Engl.* **129**, 2283–2291.

**Fischer, A. J., McGuire, C. R., Dierks, B. D. and Reh, T. A.** (2002b). Insulin and fibroblast growth factor 2 activate a neurogenic program in Müller glia of the chicken retina. *J. Neurosci. Off. J. Soc. Neurosci.* **22**, 9387–9398.

**Fischer, A. J., Schmidt, M., Schmidt, M., Omar, G. and Reh, T. A.** (2004). BMP4 and CNTF are neuroprotective and suppress damage-induced proliferation of Müller glia in the retina. *Mol. Cell. Neurosci.* **27**, 531–542.

**Fischer, A. J., Foster, S., Scott, M. A. and Sherwood, P.** (2008a). The transient expression of LIM-domain transcription factors is coincident with the delayed maturation of photoreceptors in the chicken retina. *J. Comp. Neurol.* **506**, 584–603.

**Fischer, A. J., Ritchey, E. R., Scott, M. A. and Wynne, A.** (2008b). Bullwhip neurons in the retina regulate the size and shape of the eye. *Dev. Biol.* **317**, 196–212.

**Fischer, A. J., Scott, M. A., Ritchey, E. R. and Sherwood, P.** (2009a). Mitogen-activated protein kinase-signaling regulates the ability of Müller glia to proliferate and protect retinal neurons against excitotoxicity. *Glia* **57**, 1538–1552.

**Fischer, A. J., Scott, M. A. and Tuten, W.** (2009b). Mitogen-activated protein kinase-signaling stimulates Muller glia to proliferate in acutely damaged chicken retina. *Glia* **57**, 166–81.

**Fischer, A. J., Scott, M. A., Ritchey, E. R. and Sherwood, P.** (2009c). Mitogen-activated protein kinase-signaling regulates the ability of Müller glia to proliferate and protect retinal neurons against excitotoxicity. *Glia* **57**, 1538–1552.

**Fischer, A. J., Scott, M. A., Zelinka, C. and Sherwood, P.** (2010). A novel type of glial cell in the retina is stimulated by insulin-like growth factor 1 and may exacerbate damage to neurons and Müller glia. *Glia* **58**, 633–649.

**Fischer, A. J., Zelinka, C., Gallina, D., Scott, M. A. and Todd, L.** (2014a). Reactive microglia and macrophage facilitate the formation of Müller glia-derived retinal progenitors. *Glia* **62**, 1608–1628.

**Fischer, A. J., Zelinka, C., Gallina, D., Scott, M. A. and Todd, L.** (2014b). Reactive microglia and macrophage facilitate the formation of Müller glia-derived retinal progenitors. *Glia* **62**, 1608–1628.

**Fornes, O., Castro-Mondragon, J. A., Khan, A., van der Lee, R., Zhang, X., Richmond, P. A., Modi, B. P., Correard, S., Gheorghe, M., Baranašić, D., et al.** (2020). JASPAR 2020: update of the open-access database of transcription factor binding profiles. *Nucleic Acids Res.* **48**, D87–D92.

**Furukawa, T., Mukherjee, S., Bao, Z. Z., Morrow, E. M. and Cepko, C. L.** (2000). rax, Hes1, and notch1 promote the formation of Muller glia by postnatal retinal progenitor cells. *Neuron* **26**, 383–94.

**Gallina, D., Todd, L. and Fischer, A. J.** (2014a). A comparative analysis of Müller glia-mediated regeneration in the vertebrate retina. *Exp. Eye Res.* **123**, 121–130.

**Gallina, D., Zelinka, C. and Fischer, A. J.** (2014b). Glucocorticoid receptors in the retina, Müller glia and the formation of Müller glia-derived progenitors. *Dev. Camb. Engl.* **141**, 3340–3351.

**Gallina, D., Palazzo, I., Steffenson, L., Todd, L. and Fischer, A. J.** (2016). Wnt/β-catenin-signaling and the formation of Müller glia-derived progenitors in the chick retina. *Dev. Neurobiol.* **76**, 983–1002.

**Ghai, K., Zelinka, C. and Fischer, A. J.** (2009). Serotonin released from amacrine neurons is scavenged and degraded in bipolar neurons in the retina. *J Neurochem* **111**, 1–14.

**Ghai, K., Zelinka, C. and Fischer, A. J.** (2010). Notch signaling influences neuroprotective and proliferative properties of mature Müller glia. *J. Neurosci. Off. J. Soc. Neurosci.* **30**, 3101–3112.

**Hayes, S., Nelson, B. R., Buckingham, B. and Reh, T. A.** (2007). Notch signaling regulates regeneration in the avian retina. *Dev Biol* **312**, 300–11.

**Hoang, T., Wang, J., Boyd, P., Wang, F., Santiago, C., Jiang, L., Yoo, S., Lahne, M., Todd, L. J., Jia, M., et al.** (2020). Gene regulatory networks controlling vertebrate retinal regeneration. *Science* **370**,.

**Iida, A., Iwagawa, T., Baba, Y., Satoh, S., Mochizuki, Y., Nakauchi, H., Furukawa, T., Koseki, H., Murakami, A. and Watanabe, S.** (2015). Roles of histone H3K27 trimethylase Ezh2 in retinal proliferation and differentiation. *Dev. Neurobiol.* **75**, 947–960.

**Jorstad, N. L., Wilken, M. S., Grimes, W. N., Wohl, S. G., VandenBosch, L. S., Yoshimatsu, T., Wong, R. O., Rieke, F. and Reh, T. A.** (2017). Stimulation of functional neuronal regeneration from Muller glia in adult mice. *Nature*.

**Jorstad, N. L., Wilken, M. S., Todd, L., Finkbeiner, C., Nakamura, P., Radulovich, N., Hooper, M. J., Chitsazan, A., Wilkerson, B. A., Rieke, F., et al.** (2020). STAT Signaling Modifies Ascl1 Chromatin Binding and Limits Neural Regeneration from Muller Glia in Adult Mouse Retina. *Cell Rep.* **30**, 2195-2208.e5.

**Karl, M. O., Hayes, S., Nelson, B. R., Tan, K., Buckingham, B. and Reh, T. A.** (2008). Stimulation of neural regeneration in the mouse retina. *Proc Natl Acad Sci U A* **105**, 19508–13.

**Kasinath, V., Beck, C., Sauer, P., Poepsel, S., Kosmatka, J., Faini, M., Toso, D., Aebersold, R. and Nogales, E.** (2021). JARID2 and AEBP2 regulate PRC2 in the presence of H2AK119ub1 and other histone modifications. *Science* **371**, eabc3393.

**Kong, X., Chen, L., Jiao, L., Jiang, X., Lian, F., Lu, J., Zhu, K., Du, D., Liu, J., Ding, H., et al.** (2014). Astemizole arrests the proliferation of cancer cells by disrupting the EZH2-EED interaction of polycomb repressive complex 2. *J. Med. Chem.* **57**, 9512–9521.

**Konze, K. D., Ma, A., Li, F., Barsyte-Lovejoy, D., Parton, T., Macnevin, C. J., Liu, F., Gao, C., Huang, X.-P., Kuznetsova, E., et al.** (2013). An orally bioavailable chemical probe of the Lysine Methyltransferases EZH2 and EZH1. *ACS Chem. Biol.* **8**, 1324–1334.

**Lattke, M., Goldstone, R., Ellis, J. K., Boeing, S., Jurado-Arjona, J., Marichal, N., MacRae, J. I., Berninger, B. and Guillemot, F.** (2021). Extensive transcriptional and chromatin changes underlie astrocyte maturation in vivo and in culture. *Nat. Commun.* **12**, 4335.

**Lee, M.-S., Wan, J. and Goldman, D.** (2020). Tgfb3 collaborates with PP2A and notch signaling pathways to inhibit retina regeneration. *eLife* **9**,.

**Liu, Y., Beyer, A. and Aebersold, R.** (2016). On the Dependency of Cellular Protein Levels on mRNA Abundance. *Cell* **165**, 535–550.

**Margueron, R., Trojer, P. and Reinberg, D.** (2005). The key to development: interpreting the histone code? *Curr. Opin. Genet. Dev.* **15**, 163–176.

**Meyers, J. R., Hu, L., Moses, A., Kaboli, K., Papandrea, A. and Raymond, P. A.** (2012). beta-catenin/Wnt signaling controls progenitor fate in the developing and regenerating zebrafish retina. *Neural Dev* **7**, 30.

**Miranda, T. B., Cortez, C. C., Yoo, C. B., Liang, G., Abe, M., Kelly, T. K., Marquez, V. E. and Jones, P. A.** (2009). DZNep is a global histone methylation inhibitor that reactivates developmental genes not silenced by DNA methylation. *Mol. Cancer Ther.* **8**, 1579–1588.

**Moritz, L. E. and Trievel, R. C.** (2017). Structure, mechanism, and regulation of polycomb repressive complex 2. *J Biol Chem*.

**Nelson, C. M., Ackerman, K. M., O'Hayer, P., Bailey, T. J., Gorsuch, R. A. and Hyde, D. R.** (2013). Tumor necrosis factor-alpha is produced by dying retinal neurons and is required for Muller glia proliferation during zebrafish retinal regeneration. *J Neurosci* **33**, 6524–39.

**Ooto, S., Akagi, T., Kageyama, R., Akita, J., Mandai, M., Honda, Y. and Takahashi, M.** (2004). Potential for neural regeneration after neurotoxic injury in the adult mammalian retina. *Proc Natl Acad Sci U A* **101**, 13654–9.

**Osakada, F., Ooto, S., Akagi, T., Mandai, M., Akaike, A. and Takahashi, M.** (2007). Wnt signaling promotes regeneration in the retina of adult mammals. *J Neurosci* **27**, 4210–9.

**Palazzo, I., Deistler, K., Hoang, T. V., Blackshaw, S. and Fischer, A. J.** (2019). NF-κB signaling regulates the formation of proliferating Müller glia-derived progenitor cells in the avian retina. *bioRxiv* 724260.

**Palazzo, I., Deistler, K., Hoang, T. V., Blackshaw, S. and Fischer, A. J.** (2020). NF-κB signaling regulates the formation of proliferating Müller glia-derived progenitor cells in the avian retina. *Dev. Camb. Engl.* **147**,.

**Palazzo, I., Todd, L. J., Hoang, T. V., Reh, T. A., Blackshaw, S. and Fischer, A. J.** (2021). *NFkB-signaling promotes glial reactivity and suppresses Müller glia-mediated neuron regeneration in the mammalian retina*.

**Palazzo, I., Todd, L. J., Hoang, T. V., Reh, T. A., Blackshaw, S. and Fischer, A. J.** (2022). NFkB-signaling promotes glial reactivity and suppresses Müller glia-mediated neuron regeneration in the mammalian retina. *Glia* **70**, 1380–1401.

**Pollak, J., Wilken, M. S., Ueki, Y., Cox, K. E., Sullivan, J. M., Taylor, R. J., Levine, E. M. and Reh, T. A.** (2013). ASCL1 reprograms mouse Muller glia into neurogenic retinal progenitors. *Development* **140**, 2619–31.

**Qi, W., Zhao, K., Gu, J., Huang, Y., Wang, Y., Zhang, H., Zhang, M., Zhang, J., Yu, Z., Li, L., et al.** (2017). An allosteric PRC2 inhibitor targeting the H3K27me3 binding pocket of EED. *Nat. Chem. Biol.* **13**, 381–388.

**Qiu, X., Hill, A., Packer, J., Lin, D., Ma, Y.-A. and Trapnell, C.** (2017a). Single-cell mRNA quantification and differential analysis with Census. *Nat. Methods* **14**, 309–315.

**Qiu, X., Mao, Q., Tang, Y., Wang, L., Chawla, R., Pliner, H. A. and Trapnell, C.** (2017b). Reversed graph embedding resolves complex single-cell trajectories. *Nat. Methods* **14**, 979–982.

**Ramachandran, R., Zhao, X. F. and Goldman, D.** (2011a). Ascl1a/Dkk/beta-catenin signaling pathway is necessary and glycogen synthase kinase-3beta inhibition is sufficient for zebrafish retina regeneration. *Proc Natl Acad Sci U A* **108**, 15858–63.

**Ramachandran, R., Zhao, X. F. and Goldman, D.** (2011b). Ascl1a/Dkk/beta-catenin signaling pathway is necessary and glycogen synthase kinase-3beta inhibition is sufficient for zebrafish retina regeneration. *Proc Natl Acad Sci U A* **108**, 15858–63.

**Rapicavoli, N. A., Poth, E. M., Zhu, H. and Blackshaw, S.** (2011). The long noncoding RNA Six3OS acts in trans to regulate retinal development by modulating Six3 activity. *Neural Dev* **6**, 32.

**Rompani, S. B. and Cepko, C. L.** (2010). A common progenitor for retinal astrocytes and oligodendrocytes. *J Neurosci* **30**, 4970–80.

**Rueda, E. M., Hall, B. M., Hill, M. C., Swinton, P. G., Tong, X., Martin, J. F. and Poché, R. A.** (2019). The Hippo Pathway Blocks Mammalian Retinal Müller Glial Cell Reprogramming. *Cell Rep.* **27**, 1637-1649.e6.

**Sahu, A., Devi, S., Jui, J. and Goldman, D.** (2021). Notch signaling via Hey1 and Id2b regulates Müller glia's regenerative response to retinal injury. *Glia* **69**, 2882–2898.

**Satija, R., Farrell, J. A., Gennert, D., Schier, A. F. and Regev, A.** (2015). Spatial reconstruction of single-cell gene expression data. *Nat Biotechnol* **33**, 495–502.

**Schep, A. N., Wu, B., Buenrostro, J. D. and Greenleaf, W. J.** (2017). chromVAR: inferring transcription-factor-associated accessibility from single-cell epigenomic data. *Nat. Methods* **14**, 975–978.

**Shen, C. and Vakoc, C. R.** (2015). Gain-of-function mutation of chromatin regulators as a tumorigenic mechanism and an opportunity for therapeutic intervention. *Curr Opin Oncol* **27**, 57–63.

**Stuart, T., Srivastava, A., Madad, S., Lareau, C. A. and Satija, R.** (2021). Single-cell chromatin state analysis with Signac. *Nat. Methods* **18**, 1333–1341.

**Tan, G. and Lenhard, B.** (2016). TFBSTools: an R/bioconductor package for transcription factor binding site analysis. *Bioinforma. Oxf. Engl.* **32**, 1555–1556.

**Tan, J., Yang, X., Zhuang, L., Jiang, X., Chen, W., Lee, P. L., Karuturi, R. K. M., Tan, P. B. O., Liu, E. T. and Yu, Q.** (2007). Pharmacologic disruption of Polycomb-repressive complex 2-mediated gene repression selectively induces apoptosis in cancer cells. *Genes Dev.* **21**, 1050–1063.

**Todd, L. and Fischer, A. J.** (2015). Hedgehog-signaling stimulates the formation of proliferating Müller glia-derived progenitor cells in the retina. *Development* **142**, 2610–2622.

**Todd, L. and Reh, T. A.** (2021). Comparative Biology of Vertebrate Retinal Regeneration: Restoration of Vision through Cellular Reprogramming. *Cold Spring Harb. Perspect. Biol.* a040816.

**Todd, L., Volkov, L. I., Zelinka, C., Squires, N. and Fischer, A. J.** (2015). Heparin-binding EGF-like growth factor (HB-EGF) stimulates the proliferation of Müller glia-derived progenitor cells in avian and murine retinas. *Mol. Cell. Neurosci.* **69**, 54–64.

**Todd, L., Squires, N., Suarez, L. and Fischer, A. J.** (2016a). Jak/Stat signaling regulates the proliferation and neurogenic potential of Müller glia-derived progenitor cells in the avian retina. *Sci. Rep.* **6**, 35703.

**Todd, L., Suarez, L., Squires, N., Zelinka, C. P., Gribbins, K. and Fischer, A. J.** (2016b). Comparative analysis of glucagonergic cells, glia, and the circumferential marginal zone in the reptilian retina. *J. Comp. Neurol.* **524**, 74–89.

**Todd, L., Palazzo, I., Squires, N., Mendonca, N. and Fischer, A. J.** (2017). BMP- and TGFβ-signaling regulate the formation of Müller glia-derived progenitor cells in the avian retina. *Glia* **65**, 1640–1655.

**Todd, L., Suarez, L., Quinn, C. and Fischer, A. J.** (2018). Retinoic Acid-Signaling Regulates the Proliferative and Neurogenic Capacity of Müller Glia-Derived Progenitor Cells in the Avian Retina. *Stem Cells Dayt. Ohio* **36**, 392–405.

**Todd, L., Palazzo, I., Suarez, L., Liu, X., Volkov, L., Hoang, T. V., Campbell, W. A., Blackshaw, S., Quan, N. and Fischer, A. J.** (2019). Reactive microglia and IL1β/IL-1R1-signaling mediate neuroprotection in excitotoxin-damaged mouse retina. *J. Neuroinflammation* **16**, 118.

**Todd, L., Finkbeiner, C., Wong, C. K., Hooper, M. J. and Reh, T. A.** (2020). Microglia Suppress Ascl1-Induced Retinal Regeneration in Mice. *Cell Rep.* **33**, 108507.

**Todd, L., Hooper, M. J., Haugan, A. K., Finkbeiner, C., Jorstad, N., Radulovich, N., Wong, C. K., Donaldson, P. C., Jenkins, W., Chen, Q., et al.** (2021). Efficient stimulation of retinal regeneration from Müller glia in adult mice using combinations of proneural bHLH transcription factors. *Cell Rep.* **37**, 109857.

**Trapnell, C., Roberts, A., Goff, L., Pertea, G., Kim, D., Kelley, D. R., Pimentel, H., Salzberg, S. L., Rinn, J. L. and Pachter, L.** (2012). Differential gene and transcript expression analysis of RNA-seq experiments with TopHat and Cufflinks. *Nat Protoc* **7**, 562–78.

**Trevino, A. E., Müller, F., Andersen, J., Sundaram, L., Kathiria, A., Shcherbina, A., Farh, K., Chang, H. Y., Pașca, A. M., Kundaje, A., et al.** (2021). Chromatin and gene-regulatory dynamics of the developing human cerebral cortex at single-cell resolution. *Cell* **184**, 5053-5069.e23.

**Ueki, Y., Wilken, M. S., Cox, K. E., Chipman, L., Jorstad, N., Sternhagen, K., Simic, M., Ullom, K., Nakafuku, M. and Reh, T. A.** (2015). Transgenic expression of the proneural transcription factor Ascl1 in Muller glia stimulates retinal regeneration in young mice. *Proc Natl Acad Sci U A* **112**, 13717–22.

**Ueno, K., Iwagawa, T., Ochiai, G., Koso, H., Nakauchi, H., Nagasaki, M., Suzuki, Y. and Watanabe, S.** (2017). Analysis of Muller glia specific genes and their histone modification using Hes1-promoter driven EGFP expressing mouse. *Sci Rep* **7**, 3578.

**VandenBosch, L. S., Wohl, S. G., Wilken, M. S., Hooper, M., Finkbeiner, C., Cox, K., Chipman, L. and Reh, T. A.** (2020). Developmental changes in the accessible chromatin, transcriptome and Ascl1-binding correlate with the loss in Müller Glial regenerative potential. *Sci. Rep.* **10**, 13615.

**Vizán, P., Di Croce, L. and Aranda, S.** (2021). Functional and Pathological Roles of AHCY. *Front. Cell Dev. Biol.* **9**, 654344.

**Wall, D. S., Mears, A. J., McNeill, B., Mazerolle, C., Thurig, S., Wang, Y., Kageyama, R. and Wallace, V. A.** (2009). Progenitor cell proliferation in the retina is dependent on Notch-independent Sonic hedgehog/Hes1 activity. *J Cell Biol* **184**, 101–12.

**Wan, J., Ramachandran, R. and Goldman, D.** (2012a). HB-EGF is necessary and sufficient for Muller glia dedifferentiation and retina regeneration. *Dev Cell* **22**, 334–47.

**Wan, J., Ramachandran, R. and Goldman, D.** (2012b). HB-EGF is necessary and sufficient for Muller glia dedifferentiation and retina regeneration. *Dev Cell* **22**, 334–47.

**White, D. T., Sengupta, S., Saxena, M. T., Xu, Q., Hanes, J., Ding, D., Ji, H. and Mumm, J. S.** (2017). Immunomodulation-accelerated neuronal regeneration following selective rod photoreceptor cell ablation in the zebrafish retina. *Proc. Natl. Acad. Sci. U. S. A.* **114**, E3719–E3728.

**Wilken, M. S. and Reh, T. A.** (2016). Retinal regeneration in birds and mice. *Curr Opin Genet Dev* **40**, 57–64.

**Yan, N., Cheng, L., Cho, K., Malik, M. T., Xiao, L., Guo, C., Yu, H., Zhu, R., Rao, R. C. and Chen, D. F.** (2016). Postnatal onset of retinal degeneration by loss of embryonic Ezh2 repression of Six1. *Sci Rep* **6**, 33887.

**Yao, K., Qiu, S., Tian, L., Snider, W. D., Flannery, J. G., Schaffer, D. V. and Chen, B.** (2016). Wnt Regulates Proliferation and Neurogenic Potential of Muller Glial Cells via a Lin28/let-7 miRNA-Dependent Pathway in Adult Mammalian Retinas. *Cell Rep* **17**, 165–78.

**Young, M. J., Ray, J., Whiteley, S. J., Klassen, H. and Gage, F. H.** (2000). Neuronal differentiation and morphological integration of hippocampal progenitor cells transplanted to the retina of immature and mature dystrophic rats. *Mol Cell Neurosci* **16**, 197–205.

**Zelinka, C. P., Scott, M. A., Volkov, L. and Fischer, A. J.** (2012). The reactivity, distribution and abundance of Non-astrocytic Inner Retinal Glial (NIRG) cells are regulated by microglia, acute damage, and IGF1. *PloS One* **7**, e44477.

**Zelinka, C. P., Volkov, L., Goodman, Z. A., Todd, L., Palazzo, I., Bishop, W. A. and Fischer, A. J.** (2016). mTor signaling is required for the formation of proliferating Müller glia-derived progenitor cells in the chick retina. *Dev. Camb. Engl.* **143**, 1859–1873.

**Zhang, J., Taylor, R. J., La Torre, A., Wilken, M. S., Cox, K. E., Reh, T. A. and Vetter, M. L.** (2015). Ezh2 maintains retinal progenitor proliferation, transcriptional integrity, and the timing of late differentiation. *Dev Biol* **403**, 128–38.

**Zhao, X. F., Wan, J., Powell, C., Ramachandran, R., Myers, M. G., Jr. and Goldman, D.** (2014). Leptin and IL-6 family cytokines synergize to stimulate muller glia reprogramming and retina regeneration. *Cell Rep* **9**, 272–84.

**Table 1. List of antibodies, working dilution, host, clone/catalog number and source.**

| Antibody | Dilution | Host | Clone/Catalog number | Source |
|---|---|---|---|---|
| EZH2 | | | | |
| Sox2 | 1:1000 | Goat | KOY0418121 | R&D Systems |
| Sox9 | 1:2000 | Rabbit | AB5535 | Millipore |
| CD45 | 1:300 | Mouse | HIS-C7 | Cedi Diagnostic |
| PCNA | 1:1000 | Mouse | M0879 | Dako Immunochemicals |
| Phospho-histone H3 | 1:600 | Rabbit | | |
| Neurofilament | 1:50 | Mouse | RT97 | Developmental Studies Hybridoma Bank (DSHB) |
| H3K37me3 | | Mouse | | |
| Nkx2.2 | 1:100 | Mouse | 74.5A5 | DSHB |
| cFos | | | | |
| Glutamine synthetase | 1:1000 | Mouse | 610517 | BD Biosciences |
| pS6 | 1:750 | Rabbit | #2215; Ser240/244 | Cell Signaling |
| pStat3 | 1:100 | Rabbit | 9131 | Cell Signaling |
| pSmad1/5/8 | 1:200 | Rabbit | D5B10 | Cell Signaling |
| Anti-goat IgG Alex488 | 1:1000 | Donkey | A3214 | Life Technologies |
| Anti-goat IgG Alex568 | 1:1000 | Donkey | A-11057 | Life Technologies |
| Anti-rabbit IgG Alex488 | 1:1000 | Goat | A32731 | Life Technologies |
| Anti-rabbit IgG Alex568 | 1:1000 | Goat | A-11036 | Life Technologies |
| Anti-rabbit IgG Alex647 | 1:1000 | Goat | A32733 | Life Technologies |
| Anti-mouse IgG Alex488 | 1:1000 | Goat | A32723 | Life Technologies |
| Anti-mouse IgG Alex568 | 1:1000 | Goat | A-11004 | Life Technologies |
| Anti-mouse IgG Alex647 | 1:1000 | Goat | A32728 | Life Technologies |
| Anti-Rat IgG Alexa488 | 1:1000 | Goat | A48262 | Life Technologies |

**Figure 1**. **Expression of PRC2-related genes in retinal cells following NMDA-treatment of the chick**. scRNA-seq was used to identify patterns of expression of PRC2-related genes in retinal cells. Cells were obtained from control retinas (16,381 cells), and from retinas at 24hrs (14,298 cells), 48hrs (8421 cells) and 72 hrs (18,130 cells) after NMDA-treatment (**a**). UMAP plots revealed distinct clustering of different types of retinal cells including; resting MG, 24hr activated MG, 48+72 hrs activated MG, MGPCs, oligodendrocytes, NIRG cells, retinal ganglion cells (RGCs), amacrine cells (ACs), bipolar cells (BPs), rod photoreceptors, and cone photoreceptors (**a**). MG were identified based on the expression of *GLUL*, *VIM*, *RLBP1*, and *SLC1A3* (**b**). MGPCs were identified based on the expression of *CDK1, PCNA, SPC25* and *TOP2A* (**b**). UMAP heatmap plots demonstrate patterns and levels of expression of *EZH2, EED, SET, SUZ12, JARID2* and *AEBP1* (**c**). Pseudotime trajectories for MG and MGPCs revealed branched trajectories for resting MG, proliferating MGPCs, and activated MG from 72hr after NMDA treatment largely confined to different branches and 5 different pseudotime states (**d**). Violin/scatter plots indicate significant differences (*p<0.1, **p<0.0001, ***p<<0.0001; Wilcox rank sum with Bonferoni correction) in expression levels of in MG and MGPCs in different pseutodtime states (**e**). Expression of *GLUL*, *CDK1* and PRC2-related genes are shown across stretched pseudotime in different branches, one branch ending in MGPCs and one branch ending in activated MG (**f**). Retinas were obtain from control and NMDA-treated eyes at 24, 48 and 72 hours after treatment. Sections of the retina were labeled with antibodies to EZH2 (green; **g**-**i**) and Sox9 (red, **h**) or CD45 (red; **i**). Arrows indicate the nuclei of MG, hollow arrow-heads indicate the nuclei of NIRG cells, and small double-arrows indicate the nuclei of

microglia. The calibration bar represents 50 µm (**g**-**i**). Abbreviations: TPM – transcripts per million, ONL – outer nuclear layer, INL – inner nuclear layer, IPL – inner plexiform layer, GCL – ganglion cell layer.

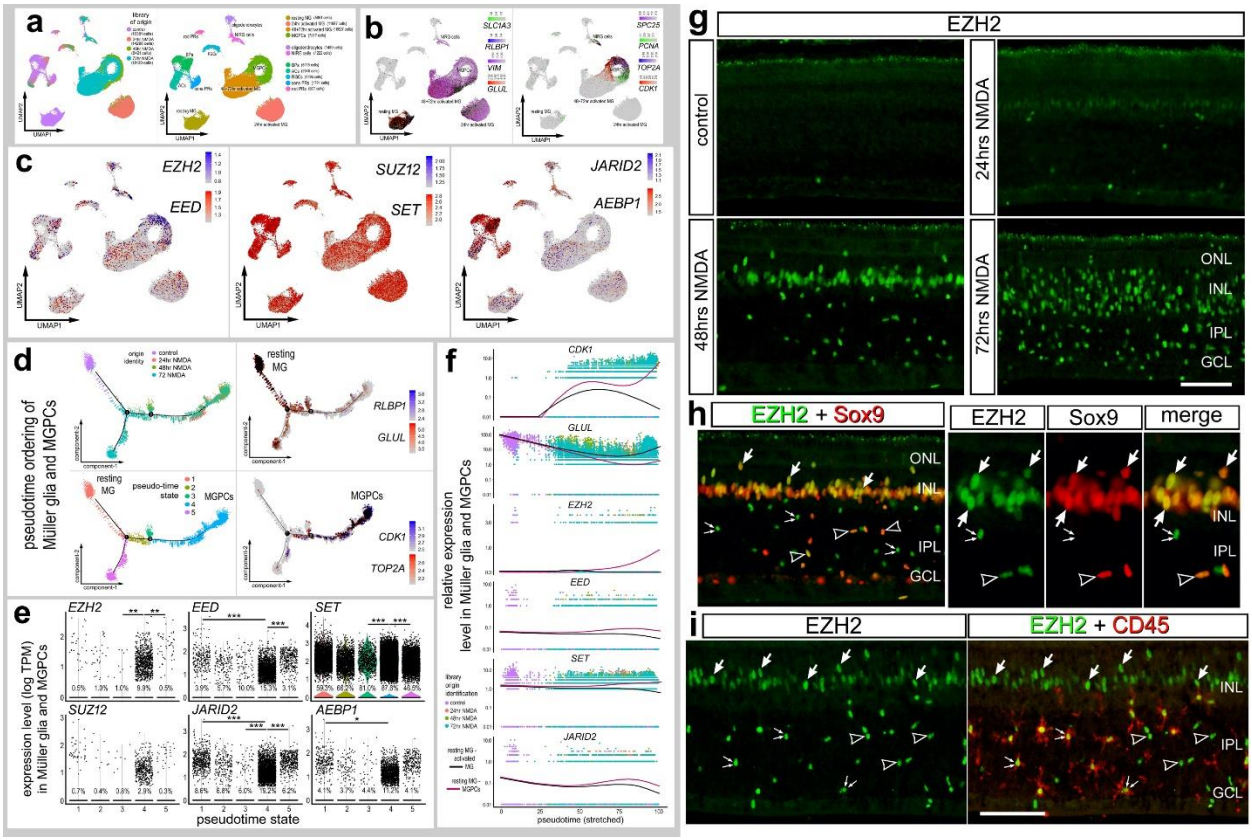

**Figure 2. Inhibition of EZH2 suppresses the proliferation of MGPCs and microglia.** Eyes were injected NMDA ± DZN (EZH2 inhibitor) at P6, EdU ± DZN at P7, P8 and P9, and retinas harvested at P10. Sections of the retina were labeled for EdU (red; **a,c,e,g**), PCNA (green; **a,c**), Sox2 (blue; **a,c**), Sox9 (green; **d**), CD45 (**e,g**), DAPI (blue; **e,g**) and TUNEL (dying cells; **h**). Histograms represent the mean (±SD) and each dot represents on biological replicate for proliferating MGPCs (**b**), proliferating and accumulating microglia (**f**), and dying cells (**i**). Significance of difference (*p<0.05, **p<0.001, ***p<0.0001) was determined using a paired t-test. Arrows indicate the nuclei of double- or triple-labeled cells. Abbreviations: ONL – outer nuclear layer, INL – inner nuclear layer, IPL – inner plexiform layer, GCL – ganglion cell layer, ns – not significant.

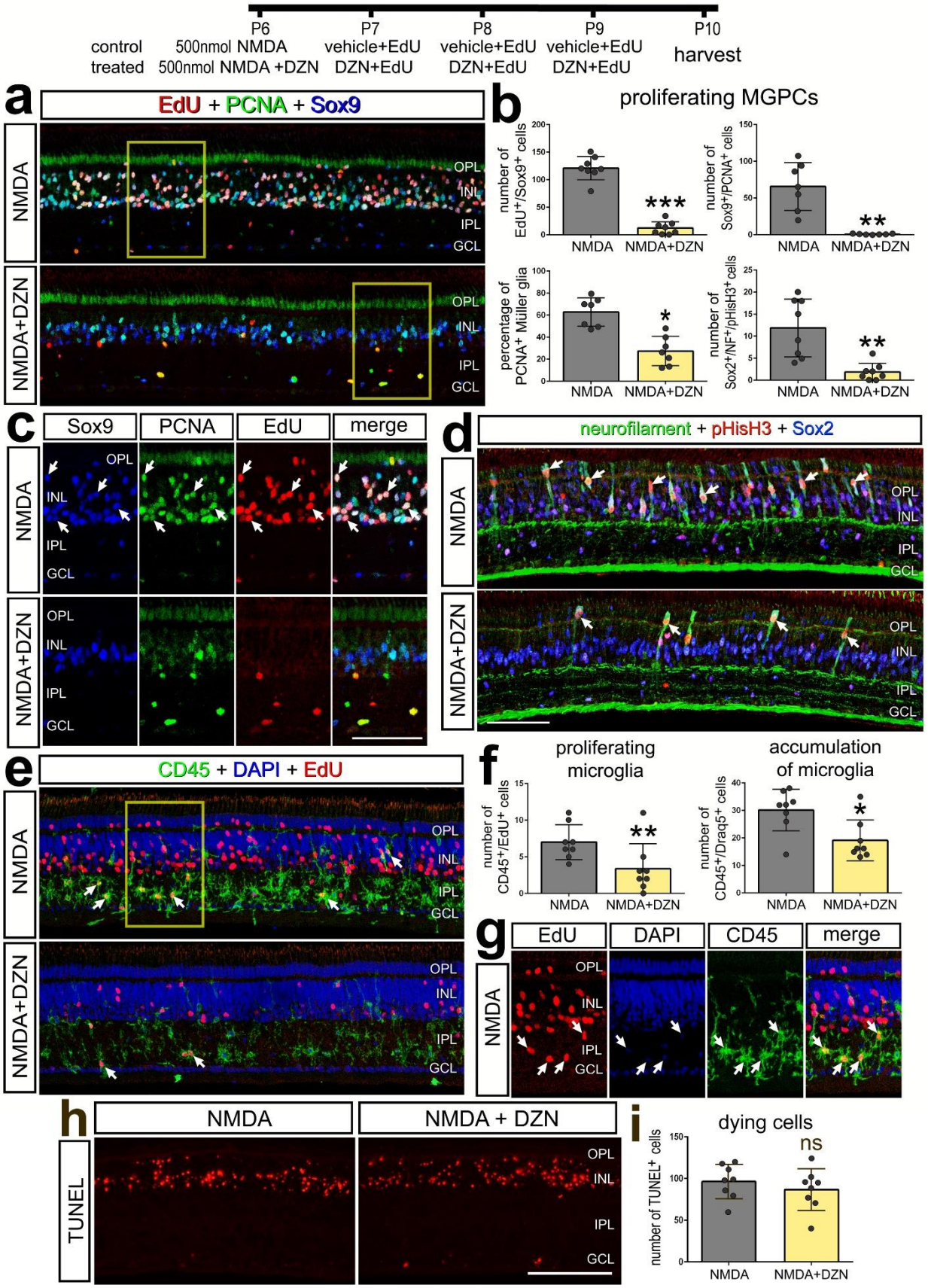

**Figure 3. Treatment of retinas with EZH2 inhibitor (DZN) reduces levels of H3K27me3 in the nuclei of MG.** Eyes were injected NMDA ± DZN (EZH2 inhibitor) at P6, EdU ± DZN at P7 and P8, and retinas harvested at 4hrs after the last injection. Sections of the retina were labeled for Sox9 (red; **a**) and H3K27me3 (green; **a**). The area boxed-out in yellow in the upper panels is enlarged 3-fold in panels below (**a**) The area occupied by Sox9 (MG nuclei) was selected and the H3K27me3 immunofluorescence cut and projected onto a greyscale background for quantification (**a**). Histograms represent the mean (±SD) and each dot represents on biological replicate for H3K27me3 levels for area (**b**), mean intensity per nuclei (**c**), and density sum (**d**) in the nuclei of MG. Significance of difference was determined using a paired t-test. Abbreviations: ONL – outer nuclear layer, INL – inner nuclear layer, IPL – inner plexiform layer, GCL – ganglion cell layer. The calibration bar in **a** represent 50 µm.

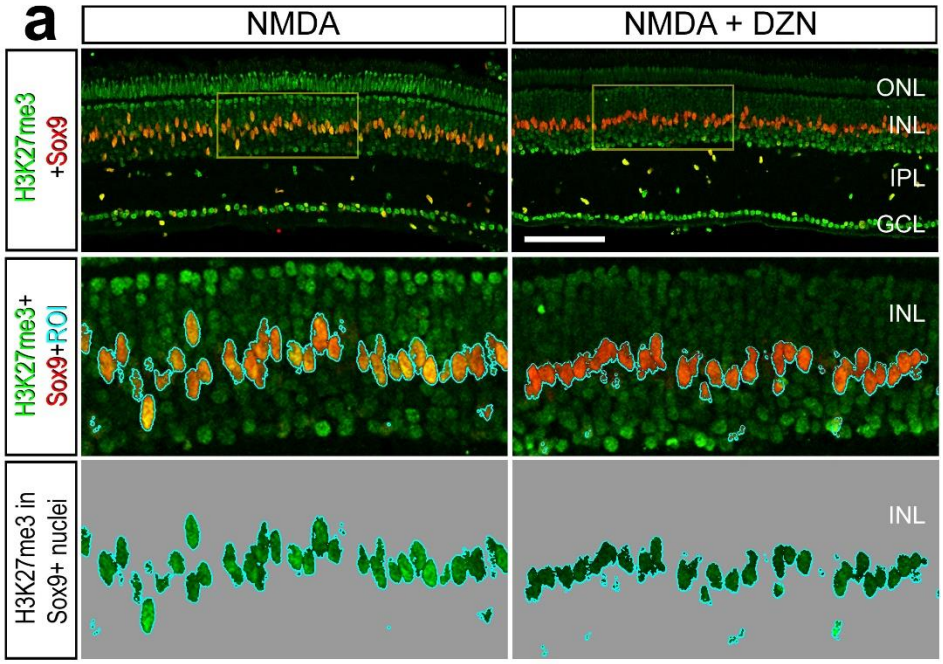


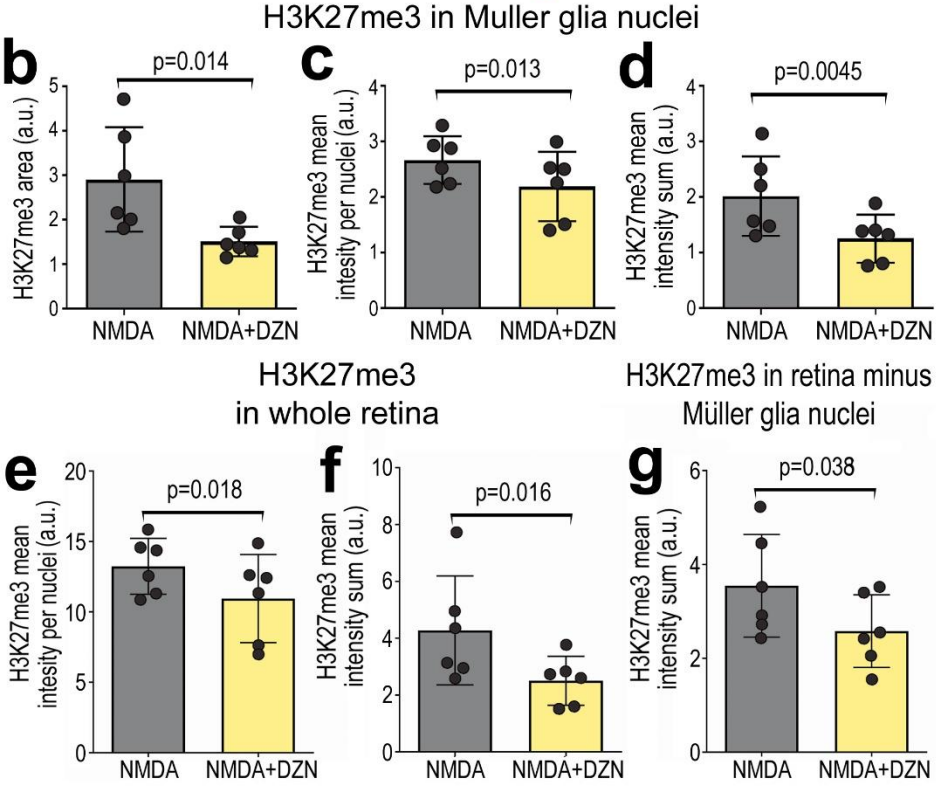

**Figure 4. Treatment of retinas with inhibitors to EED and JARID2 suppress the proliferation of MGPCs.** Eyes were injected NMDA ± inhibitor at P6, EdU ± inhibitor at P7, P8 and P9, and retinas harvested at P10. Inhibitors included UNC1999 (EZH2 inhibitor), EEDi (EED inhibitor), astemizole (EED inhibitor) and Jib04 (JMJD inhibitor). Sections of the retina were labeled for EdU (red; **a,e,f**), Sox9 (green; **a**), TUNEL (dying cells; **c**), and CD45 (**e,g**). Histograms represent the mean percentage change (±SD) for MGPC proliferation (**b**), dying cells (**d**), and microglia proliferation (**g**). Each dot represents one biological replicate. Significance of difference (*p<0.05, **p<0.001, ***p<0.0001) was determined using a paired t-test. Arrows indicate the nuclei of double-labeled cells. Abbreviations: ONL – outer nuclear layer, INL – inner nuclear layer, IPL – inner plexiform layer, GCL – ganglion cell layer, ns – not significant. The calibration bars in **a,c,e** and **f** represent 50 µm.

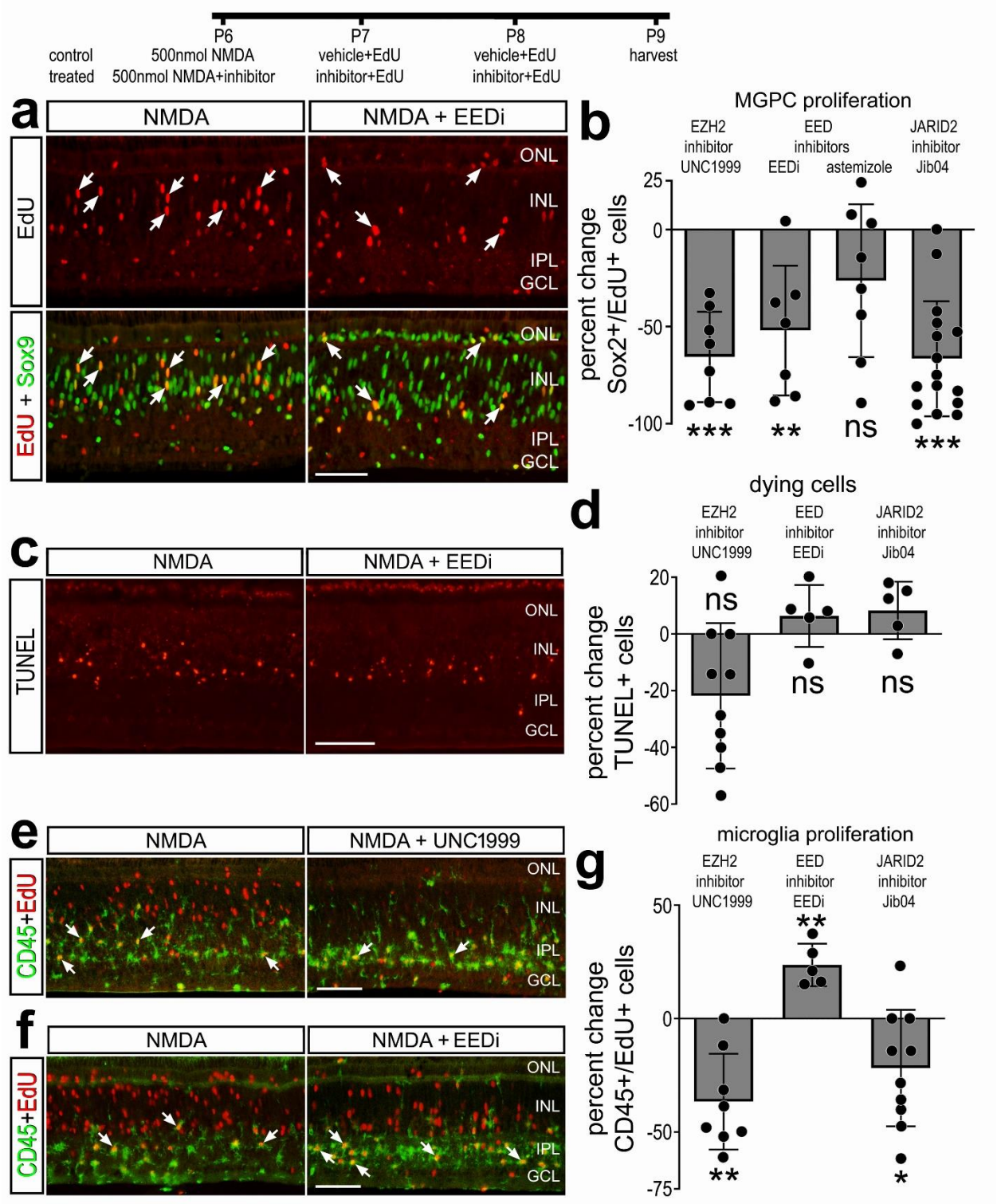

**Figure 5. Treatment of retinas with EZH2 inhibitor (DZN) influences chromatin access in MG.** Eyes were injected with saline ± DZN or NMDA ± DZN, retinas were harvested 24hrs after the last injection and scATAC-seq libraries were generated (**a**). UMAP plots were generated and clusters of cells identified based on chromatin access for genes known to be associated with retinal cell types (**b**,**c**). Genes with enhanced chromatin access in distinct cells types included *GNAT2* (cone PRs), *ISL2* and *POU4F2* (RGCs), *VSX2* (bipolar cells), *PAX6* (amacrine and horizontal cells), *TFAP2A* (amacrine cells), and illustrated in a dot plot (**c**). MG were isolated and re-ordered in UMAP plots (**d**). UMAP clusters of MG formed for resting MG (saline and saline+DZN-treated cells) and activated MG (NMDA and NMDA+DZN-treated cells) (**d**). Lists of genes with differential accessible chromatin regions (DACRs; supplemental tables 1 and 2) were generated and a The Venn diagram (**e**) constructed to illustrate numbers of genes with significantly up- and down-regulated chromatin access according to treatment. Significance of difference ($p<0.05$) was determined by using a Wilcox rank sum test with Bonferroni correction. Clusters or resting and activated MG were distinguished based on differential chromatin access to genes such as *GLUL, TGFB2* (**f,g**)*, EGR1, FOSB, FOS, CDKN1A* and *HEYL* (**h,i**). Lists of genes with differential chromatin access were applied to GO enrichment analysis (**j,k**). GO analysis was performed for gene with differential chromatin access when comparing MG from retinas treated with saline vs DZN+saline (**j**) saline vs NMDA (**k**) and. P values, GO categories and numbers of genes in each category are included for gene modules with increased or decreased chromatin access.

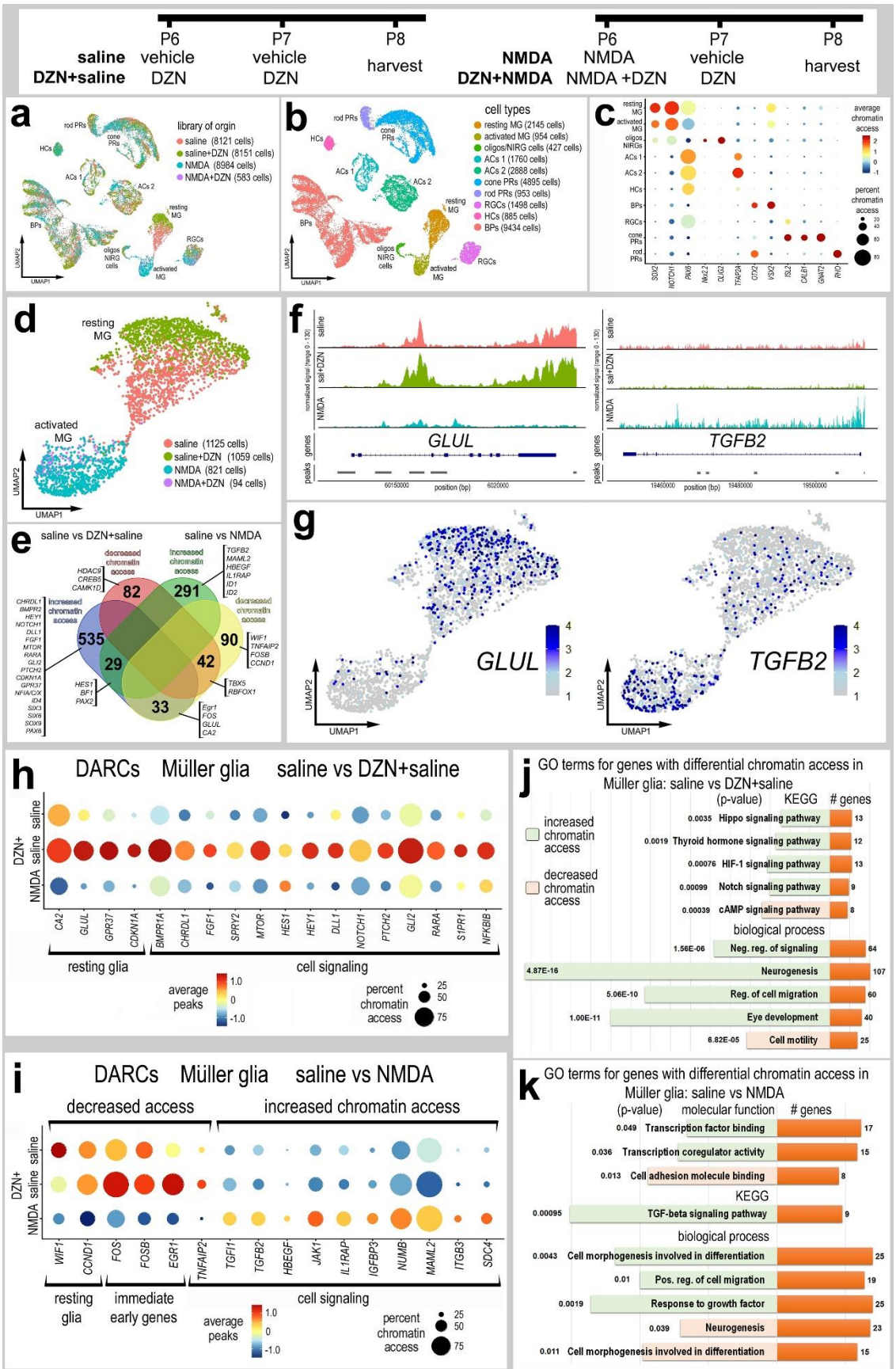

**Figure 6. Treatment of retinas with EZH2 inhibitor (DZN) and NMDA influences gene expression in MG.** Retinas were treated with saline ± DZN or NMDA ± DZN, and scRNA seq libraries were generated. UMAP plots were generated and clusters of cells identified based on established markers (**a**,**b**). MG were identified based on expression of genes associated with resting glia (**c**), activated glia (**d**) and proliferating MGPCs (**e**). Lists of DEGs were generated (supplemental table 3) for MG from retinas treated with saline vs DZN-saline, saline vs NMDA, and NMDA vs DZN-NMDA and plotted in a Venn diagram (**f**). UMAP clustered MG were isolated and analyzed for occupancy according to library of origin (**g**,**h**,**i**). MGPCs were identified based on high levels of expression of *SPC25, PCNA, TOP2A* and *CDK1* (**j**). Dot plots illustrate the percentage of expressing MG (size) and significant ($p<0.001$) changes in expression levels (heatmap) for genes in MG from retinas treated with saline vs saline-DZN (**k**) and NMDA vs NMDA-DZN (**l**). Genes related to resting MG, cell signaling, chromatin remodeling, cell cycle regulation or transcription factors (TFs) were up- or down-regulated (**k**,**l**). GO enrichment analysis was performed for lists of DEGs in MG for retinas treated with saline ± DZN and NMDA ± DZN (**n,o**). Gene modules for upregulated (green) and downregulated (peach) genes were grouped by GO category with P values and numbers of genes for each category (**n,o**).

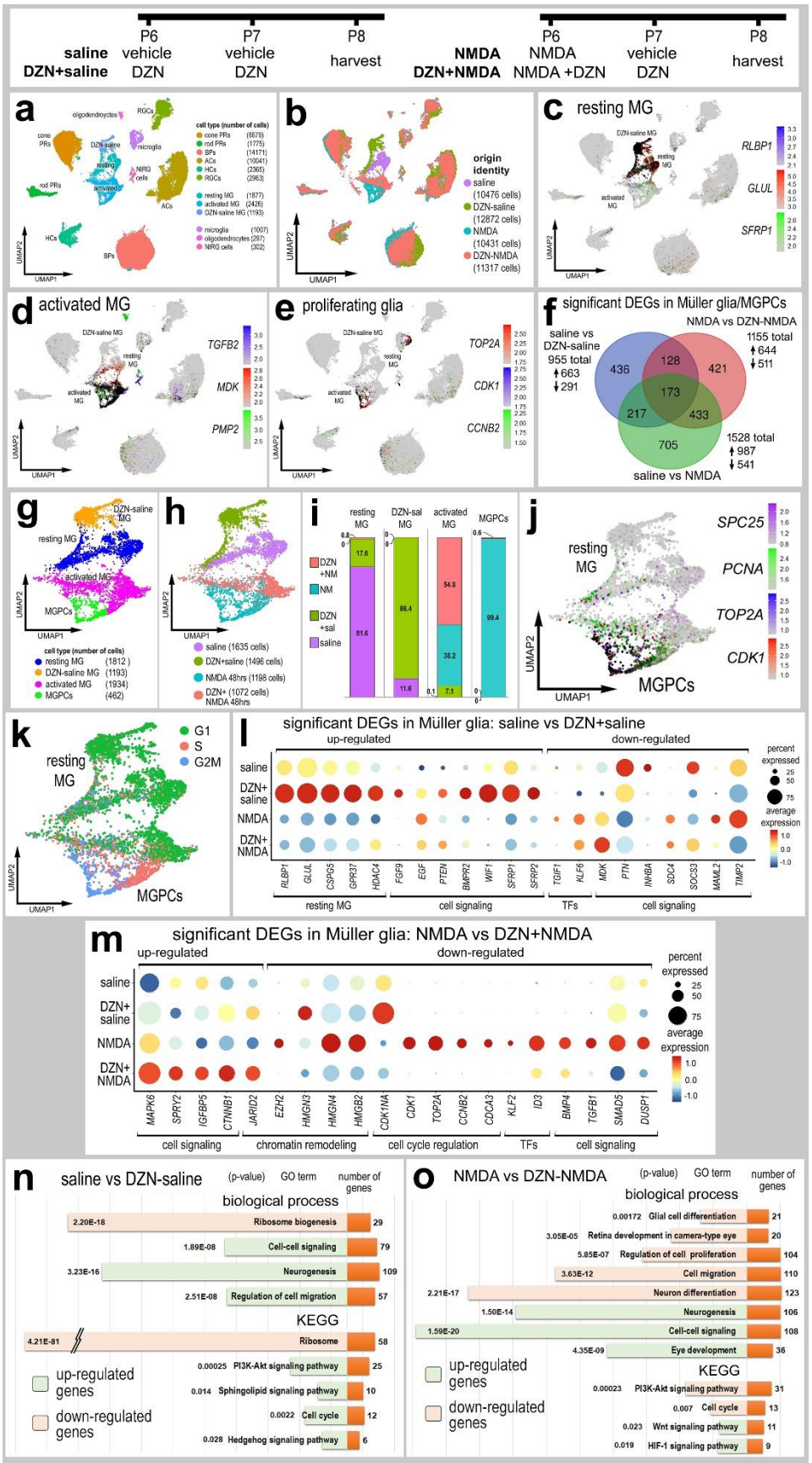

**Figure 7. Comparison of differentially expressed genes (DEGs), differentially accessible chromatin regions (DACRs) and access to transcription factor binding motifs in MG.** Venn diagrams illustrate numbers of genes with increased or decreased expression levels or chromatin access in MG from retinas treated with saline vs saline+DZN (**a**) or saline vs NMDA (**b**). UMAP heatmap plot in **c** illustrates access to SOX9 DNA-binding motifs across all types of retinal cells. Motifs enriched in activated and resting MG were identified, and included motifs for transcriptional effectors of cell signaling pathways (**d-h**). UMAP heatmap plots for MG illustrate differential access to motifs for FOS::JUN, SMAD2::SMAD2 and STAT3 in resting and activated MG (**e-g**). Dot plots illustrate heatmaps for levels of access and percent of cells with access for transcriptional effectors of cell signaling pathways (**h**) or transcription factors (**i**). For direct comparison with motif access, dot plots illustrate levels of chromatin access (**j**) and mRNA (**k**) for key transcription factors.

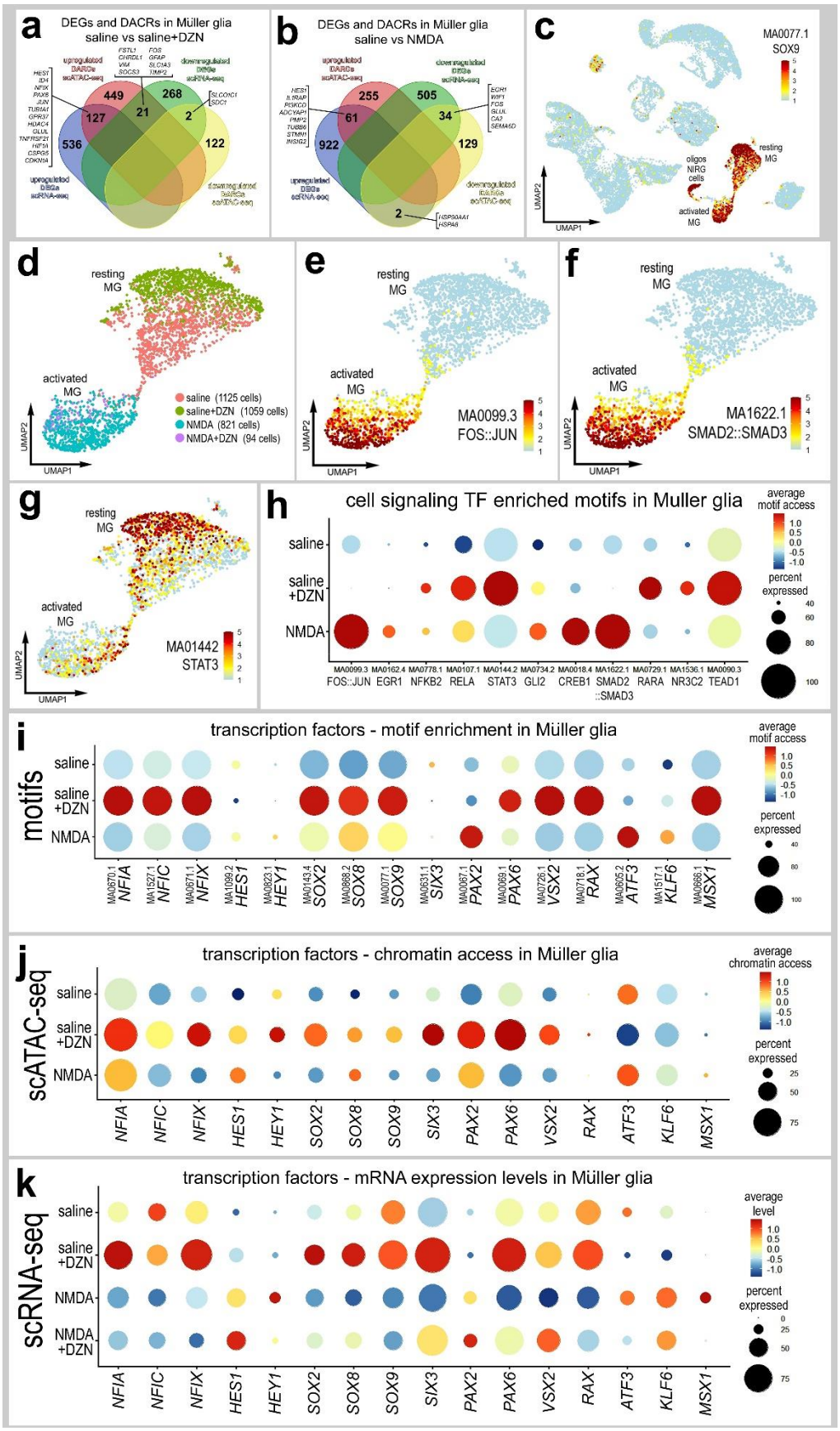

**Figure 8. Ligand-receptor (LR) interactions inferred from scRNA-seq data between microglia and MG.** Retinal microglia and MG were isolated, re-embedded and ordered in UMAP plots (**a,b**). Treatment groups included saline, saline + DZN, NMDA and NMDA + DZN. Cells were identified based on cell-distinguishing markers: Resting MG - *GLUL, GPR37, RLBP1* (**c**); reactive MG – *MDK, HBEGF, TGFB2* (**d**); microglia - *C1QA, SPI1, CSF1R* (**e**); proliferating cells (microglia and MPGCs) - *TOP2A, SPC25, CDK1* (**f**). Glia from different treatment groups were analyzed using SingleCellSignalR to generate chord diagrams and illustrate numbers of autocrine and paracrine LR-interactions (**g**). The LRscore, with the most significant LR-interactions approaching a value of 1, utilizes the mean normalized read count matrix to regularize the Ligand and Receptor read counts independent of dataset depth. Paracrine LR-interactions were identified for glial cells for different treatment groups including saline (**h**), DZN-saline (**i**), NMDA (**j**) and DZN-NMDA (**k**). For each treatment group, the 40 most significant LR-interactions between microglia and MG were identified and illustrated in chord plots with LR score heat maps (**h-k**). Treatment-specific differences in glial paracrine LR-interactions in saline vs saline + DZN (**l**) and NMDA vs NMDA +DZN (**m**) are illustrated in Venn diagrams with select interactions. Treatment-specific differences in glial autocrine LR-interactions in MG in saline vs saline + DZN (**n**) and NMDA vs NMDA +DZN (**o**) are illustrated in Venn diagrams with select interactions.

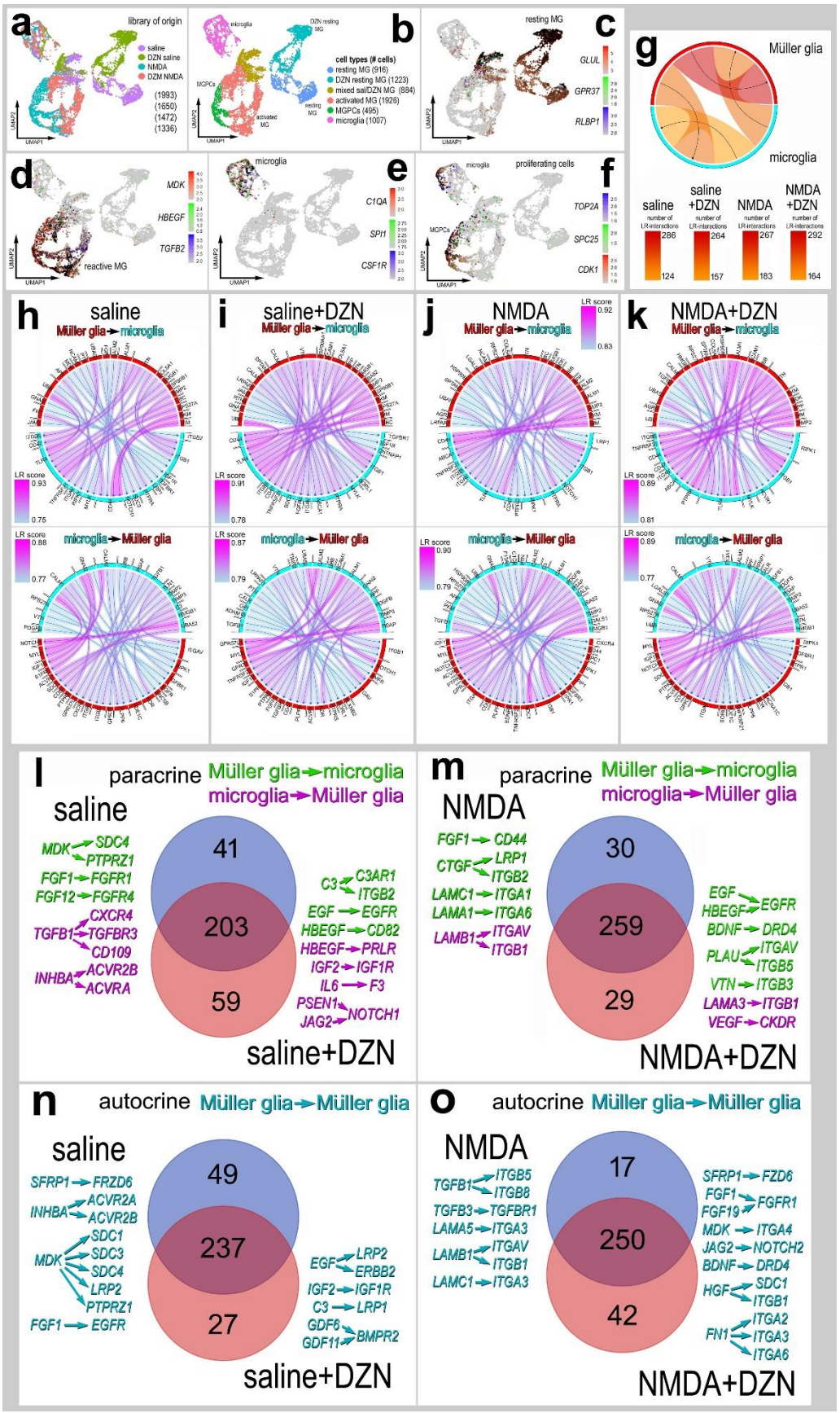

**Figure 9. Cell signaling in MG in damaged retinas is influenced by inhibition of EZH2.** Eyes were injected with NMDA ± DZN (EZH2 inhibitor) at P6, vehicle or DZN at P7, and eyes harvested at 4 hrs after the last injection. Retinal sections were for cell death (TUNEL) or antibodies to cFos and Sox2, pS6 and pStat3 (**a**). The calibration bars in **a** represent 50 µm. (**b**-**f**) Histograms represent the mean (±SD) and each dot represents one biological replicate. Significance of difference (p-value) was determined using a paired t-test. Abbreviations: ONL – outer nuclear layer, INL – inner nuclear layer, IPL – inner plexiform layer, GCL – ganglion cell layer, ns – not significant.

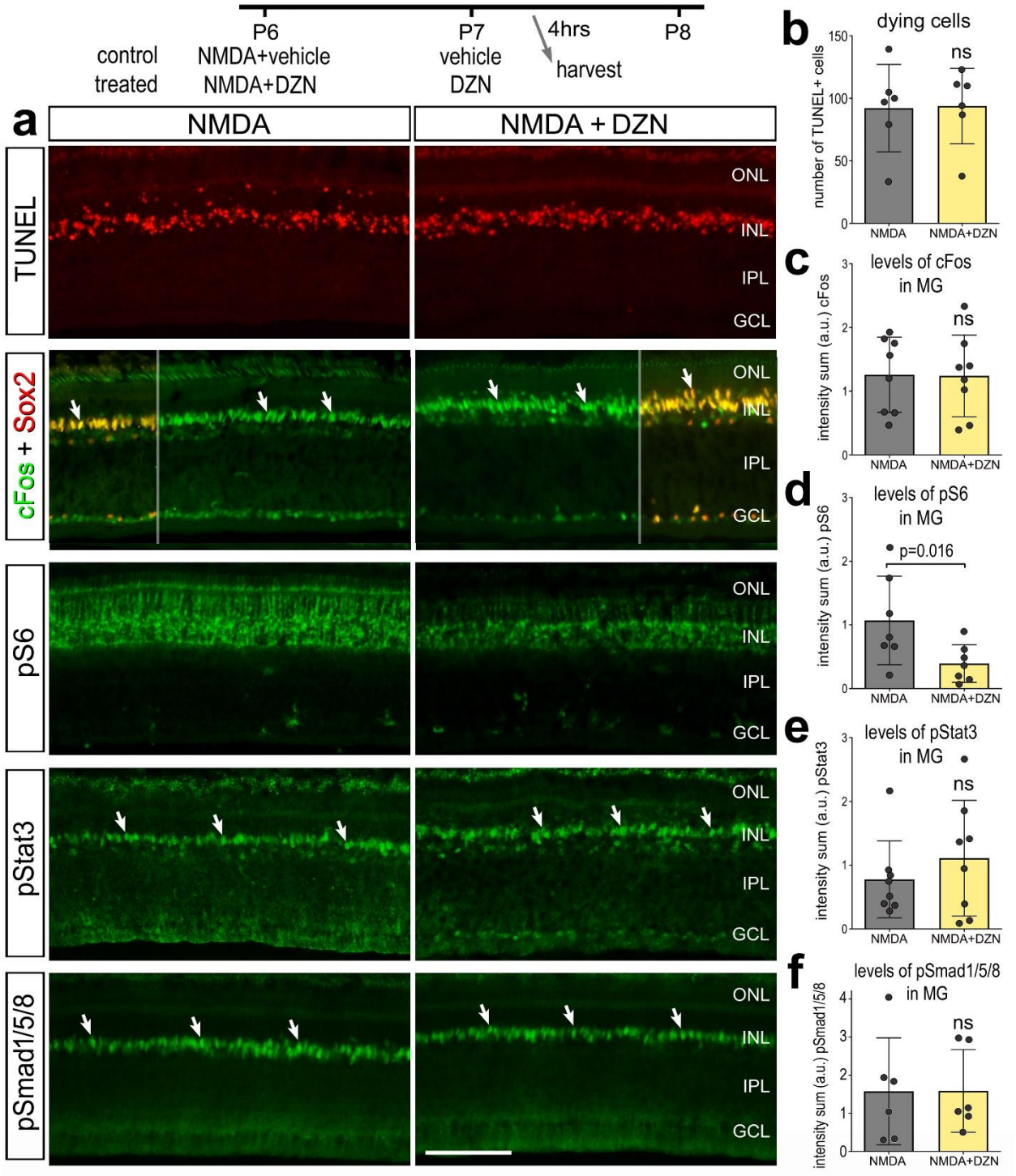

**Figure 10. EZH2 inhibition in retinas treated with insulin + FGF2 suppresses the proliferation of MGPCs and CMZ progenitors.** Eyes were injected with insulin+FGF2+EdU ± DZN at P7, P8 and P9, EdU at P10 and P11, and retinas harvested 24 hrs after the last injection. Sections of the retina were labeled for EdU (red; **b, i, k**), or antibodies to EZH2 (green; **a**), Sox2 (green; **b,f, i, k**; blue; **d**), pHisH3 (red; **d**), cFos (green; **h**), pSmad1/5/8 (green; **h**), or pStat3 (green; **h**). Sections of the far peripheral retina and CMZ were labeled for EdU (red) and Sox2 (green). White arrows indicate the nuclei of MG and blue arrows indicate nuclei in the CMZ that are double-labeled for EdU and Sox2. The calibration bars represent 50 µm. (**c**, **e, g, j**) Histograms represent the mean (±SD) and each dot represents one biological replicate. Significance of difference was determined using a Mann-Whitney U test (**c,e**), ANOVA (**g**), or paired t-test (**j**). Abbreviations: NPE – non-pigmented epithelium, CMZ – circumferential marginal zone, ONL – outer nuclear layer, INL – inner nuclear layer, IPL – inner plexiform layer, GCL – ganglion cell layer.

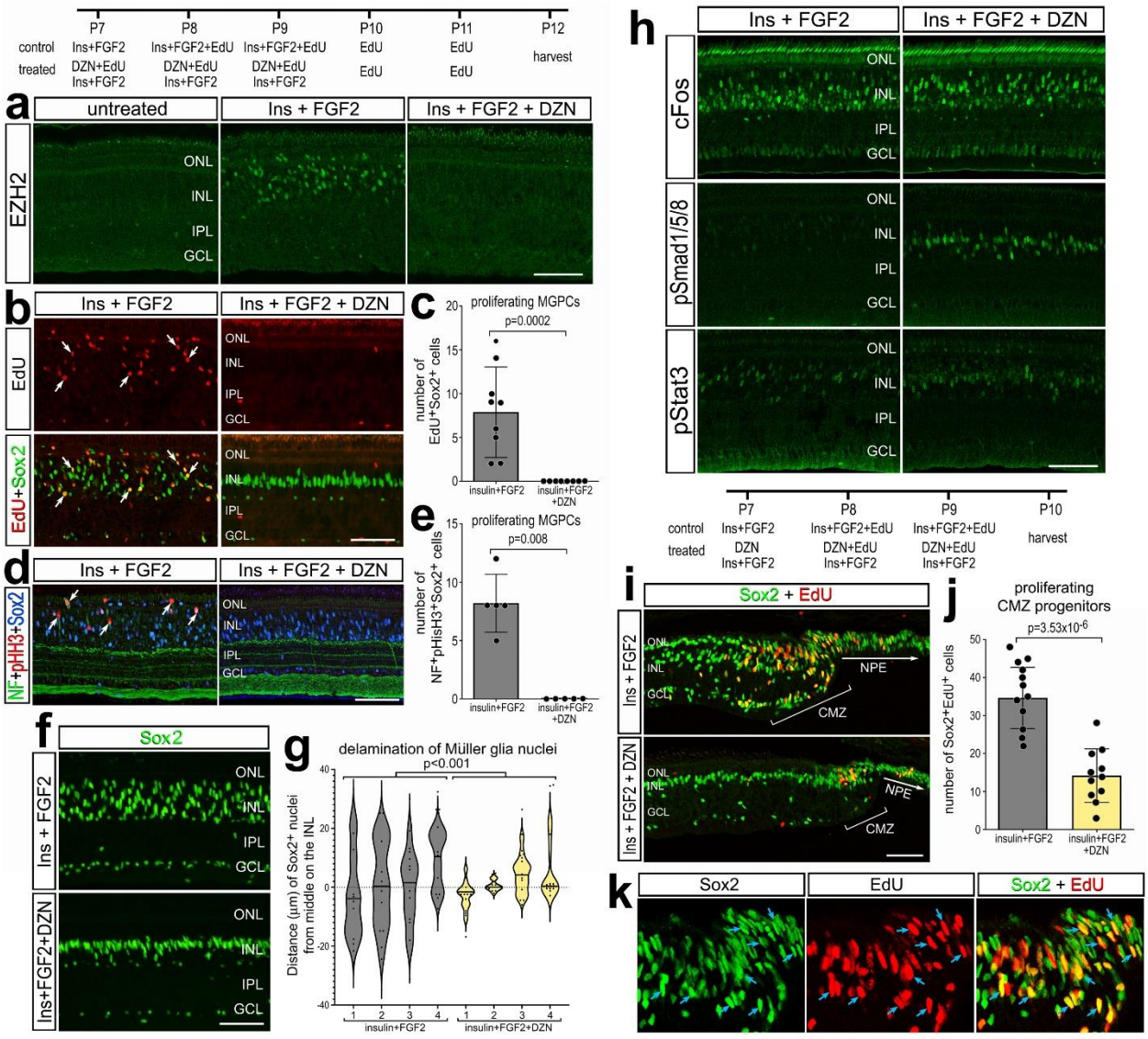

**Figure 11. PRC2 related genes in normal and damaged mouse retinas.** UMAP plots of aggregated scRNA-seq libraries prepared from control retinas and retinas 3, 6, 12, 24, 36, 48, and 72 hours after NMDA damage; numbers of cells per library or per cluster in parentheses (**a**). Clusters of different types of retinal cells were identified based on collective expression of different cell-distinguishing markers as described in the Materials and Methods (**b**). Resting MG and reactive MG identified by expression of *Slc1a3* or *Nes and Vim,* respectively (**c**). UMAP heatmap plots illustrate patterns and expression levels of *Ezh2, Eed, Set, Suz12, Jarid2* and *Aebp2* across all retinal cells (**d-f**). MG were isolated and re-embedded in UMAP plots to reveal distinct clusters of resting and activated MG (**g**). Violin/scatter plots illustrate expression levels of PRC2-related genes within MG (**h**). Significance of difference (**p<0.01, **p<0.0001, ***p<<0.0001) was determined by using a Wilcoxon rank sum with Bonferroni correction. **EZH2 inhibitor has no effect upon the differentiation of neurons from *Ascl1*-overexpressing MG.** (**i-l**) Tamoxifen was administered IP 1x daily for 4 consecutive days to *Glast-CreER:LNL-tTA:tetO-mAscl1-ires-GFP* mice. NMDA was injected intravitreally in left (control) eyes and NMDA + DZN in right (treated) eyes on D8, vehicle ± DZN on D9, vehicle ± DZN on D10, and retinas were harvested 2 weeks after the last injection. Retinal sections were labeled for GFP (green), and Sox2 (red; **i**) or Otx2 (red; **j**). Arrows in **i** and **j** indicate cells double-labeled for GFP and Sox2 or Otx2. Histograms illustrate the mean percentage (±SD and individual data points) of $GFP^+$ cells that are $Sox2^+$ (**k**) or $Otx2^+$ (**l**). Significance of difference (p-values shown) was determined by using a paired t-test. The calibration bar in **j** represents 50 µm.

Abbreviations: ONL, outer nuclear layer; INL, inner nuclear layer; GCL, ganglion cell layer.

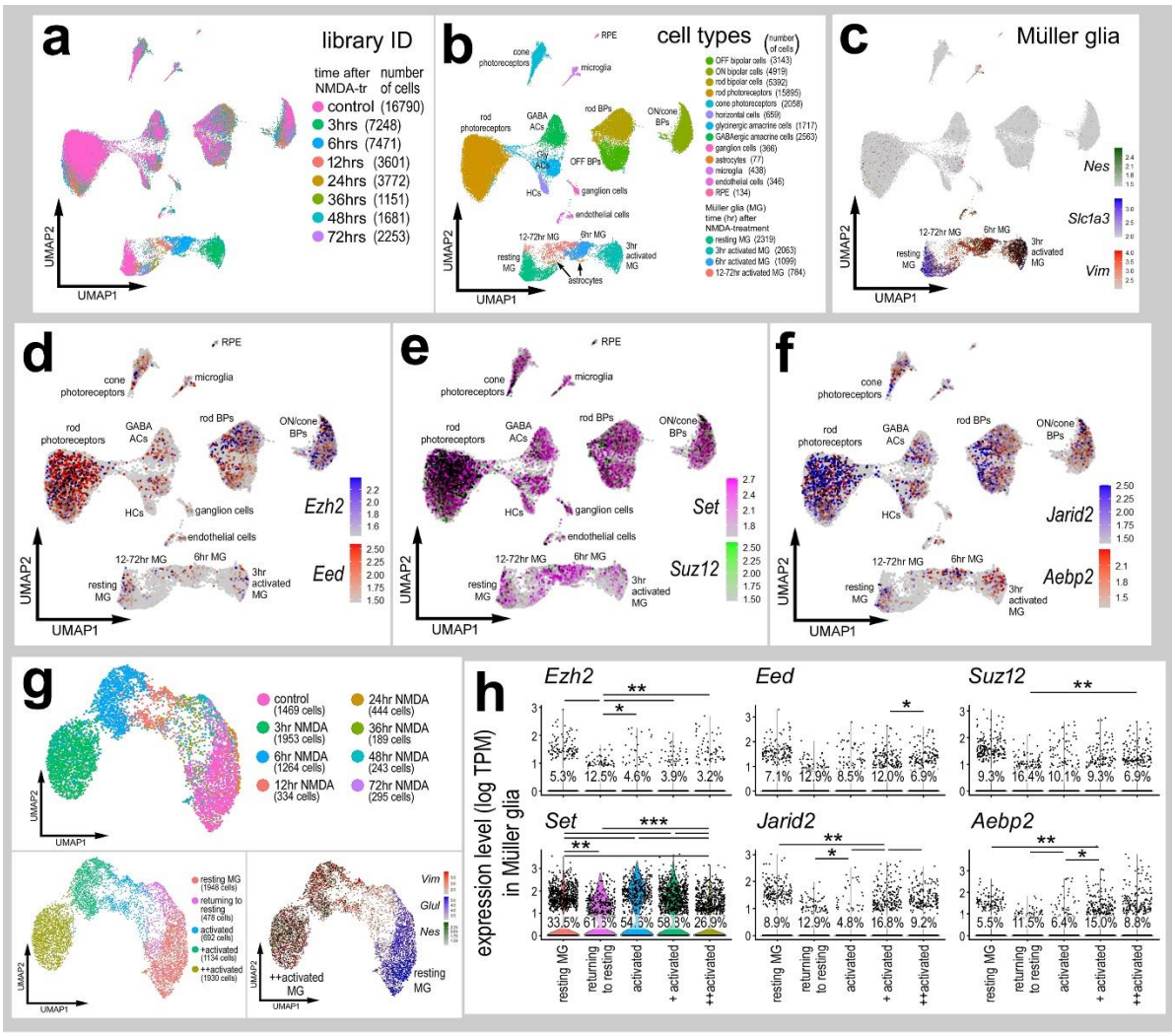


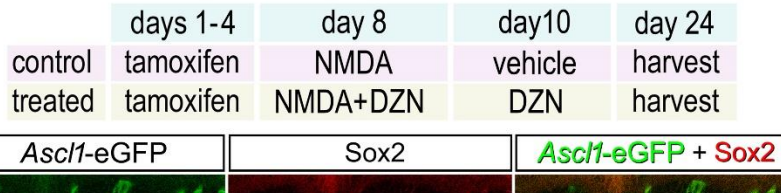


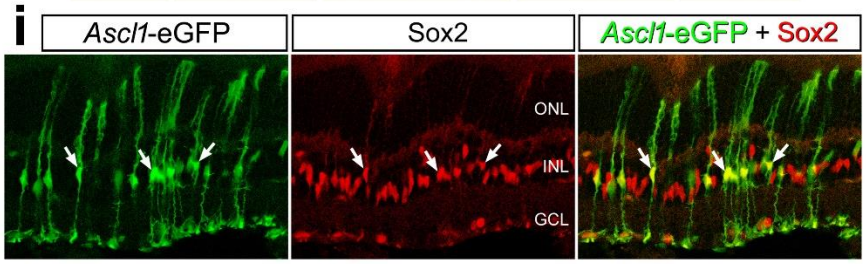


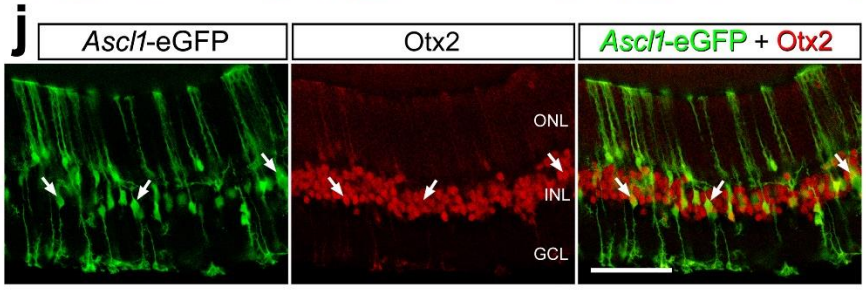


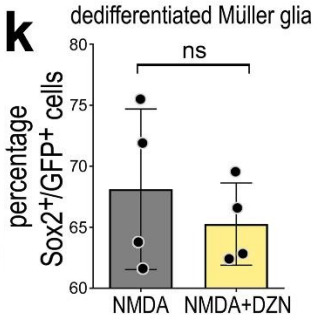


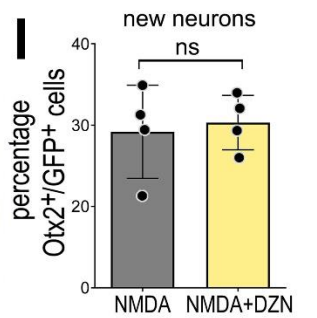

**Figure 12. Schematic summary of actions of EZH2-, EED- and JARID2-inhibitors on microglia, MG, NIRG cells and neurons.**

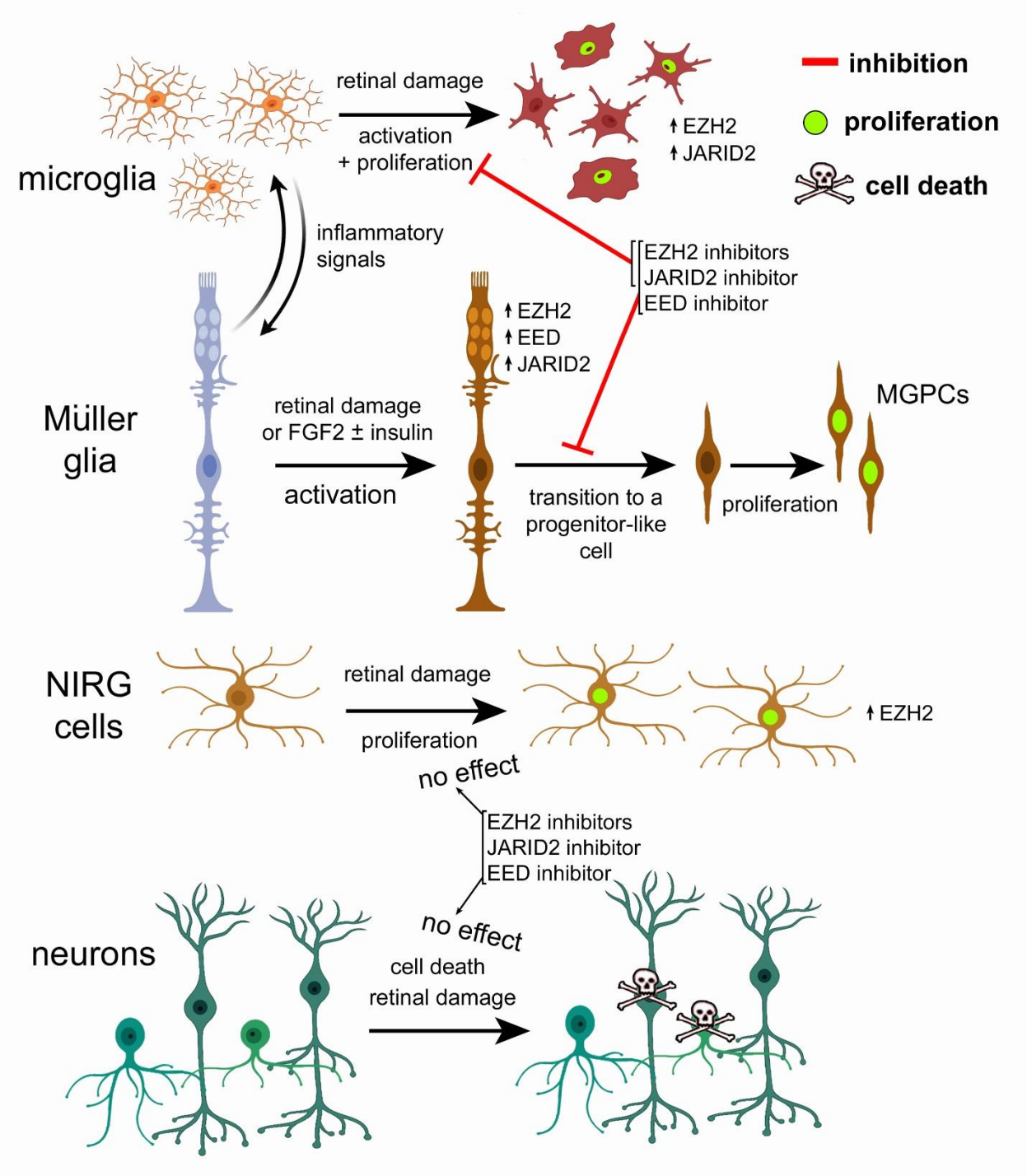

**Supplemental Figure 1. Expression of PRC2-related genes in resting and activated microglia.** scRNA-seq was used to identify patterns of gene expression among microglia in control and NMDA-damaged retinas. In UMAP plots (**a**-**e**) and violin plots (**g**) each dot represents one cell. Cells were obtained from control retinas (309 cells) or at different times after NMDA-treatment including 3 hrs (143 cells), 12 hrs (408 cells) and 48hrs (261 cells) (**a**). UMAP plots revealed distinct clustering of different types of microglia including resting (245 cells), early activated (344), activated (117), and late activated (415 cells). UMAP heatmap illustrate the distribution and levels of genes in resting and early activated microglia (*TNFSF15, PPARG, IL1R2;* **c**) and activated/late activated microglia (*DBI, AIF1L;* **d**). UMAP heatmap (**f,e**) and violin plots (**g**) illustrate the distribution and levels of expression of PRC2-related genes: *EZH2, EED, SET, RBBP4, JARID2* and *AEBP1*. Violin/scatter plots indicate significant differences (*p<0.01, **p<0.0001; Wilcox rank sum with Bonferoni correction) in expression levels of in microglia (**g**).

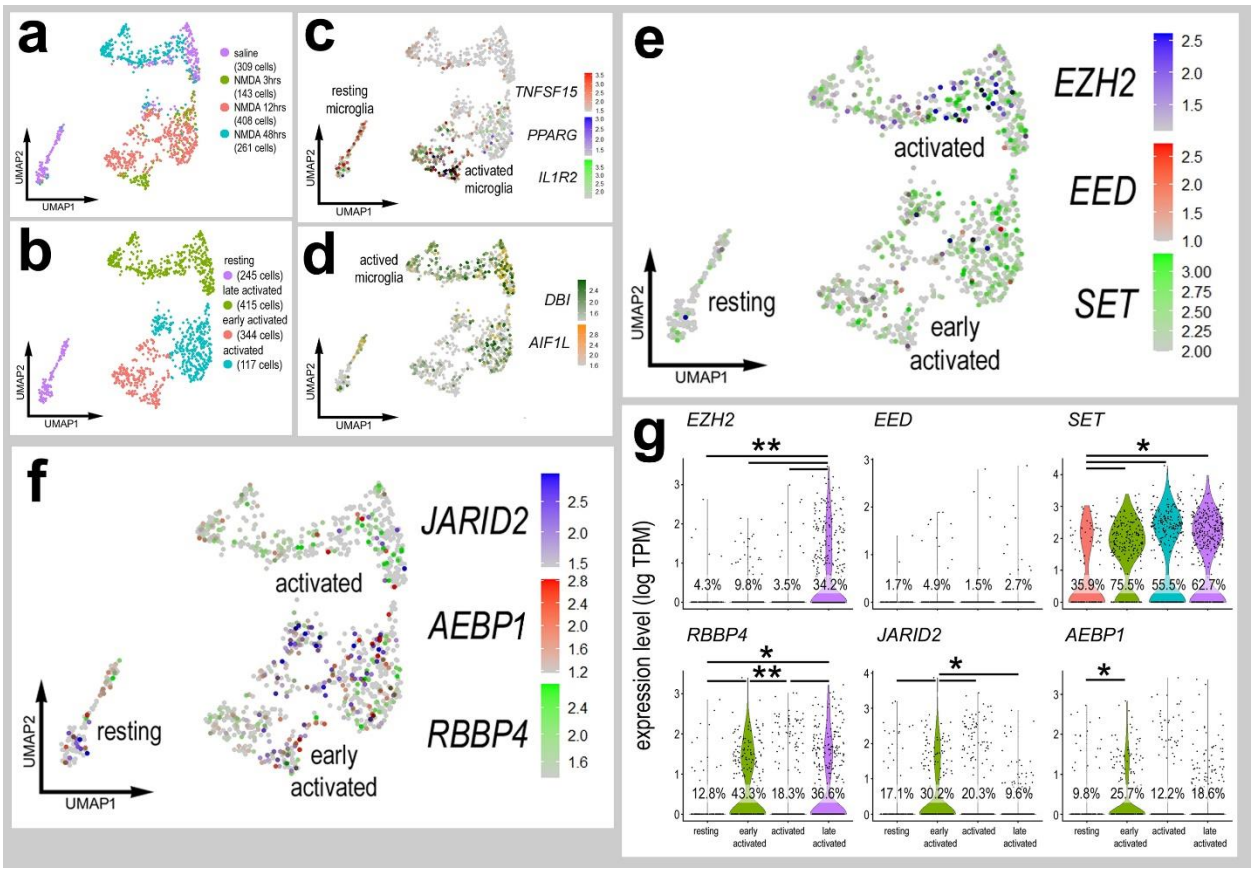

**Supplemental Figure 2. NIRG cells, cell death and numbers of MG are unaffected by EZH2 inhibitor.** (**a**-**b**) Eyes were injected with NMDA ± DZN (EZH2 inhibitor) at P6, EdU ± DZN at P7, P8 and P9, and retinas harvested at P10. Sections of the retina were labeled for EdU (blue - **a**), Nkx2.2 (green – **a**) and Sox9 (red - **a**). (**c**-**e**) Eyes were injected with vehicle or DZN at P6, P7 and P8, and eyes were harvested at P9. Sections of the retina were labeled for dying cells (TUNEL - **c**) or Sox9 (green – **d**). Histograms represent the mean (±SD) and each dot represents on biological replicate for numbers of NIRG cells (**b**) or numbers of $Sox9^+$ MG (**d**). Significance of difference (*$p<0.05$, ns – not significant) was determined using a paired t-test (**b**) or ANOVA with post-hoc t-test with Bonferroni correction (**e**). Arrows indicate the nuclei of MG and hollow arrowheads indicated the nuclei of NIRG cells (**a,d**). Abbreviations: ONL – outer nuclear layer, INL – inner nuclear layer, IPL – inner plexiform layer, GCL – ganglion cell layer.

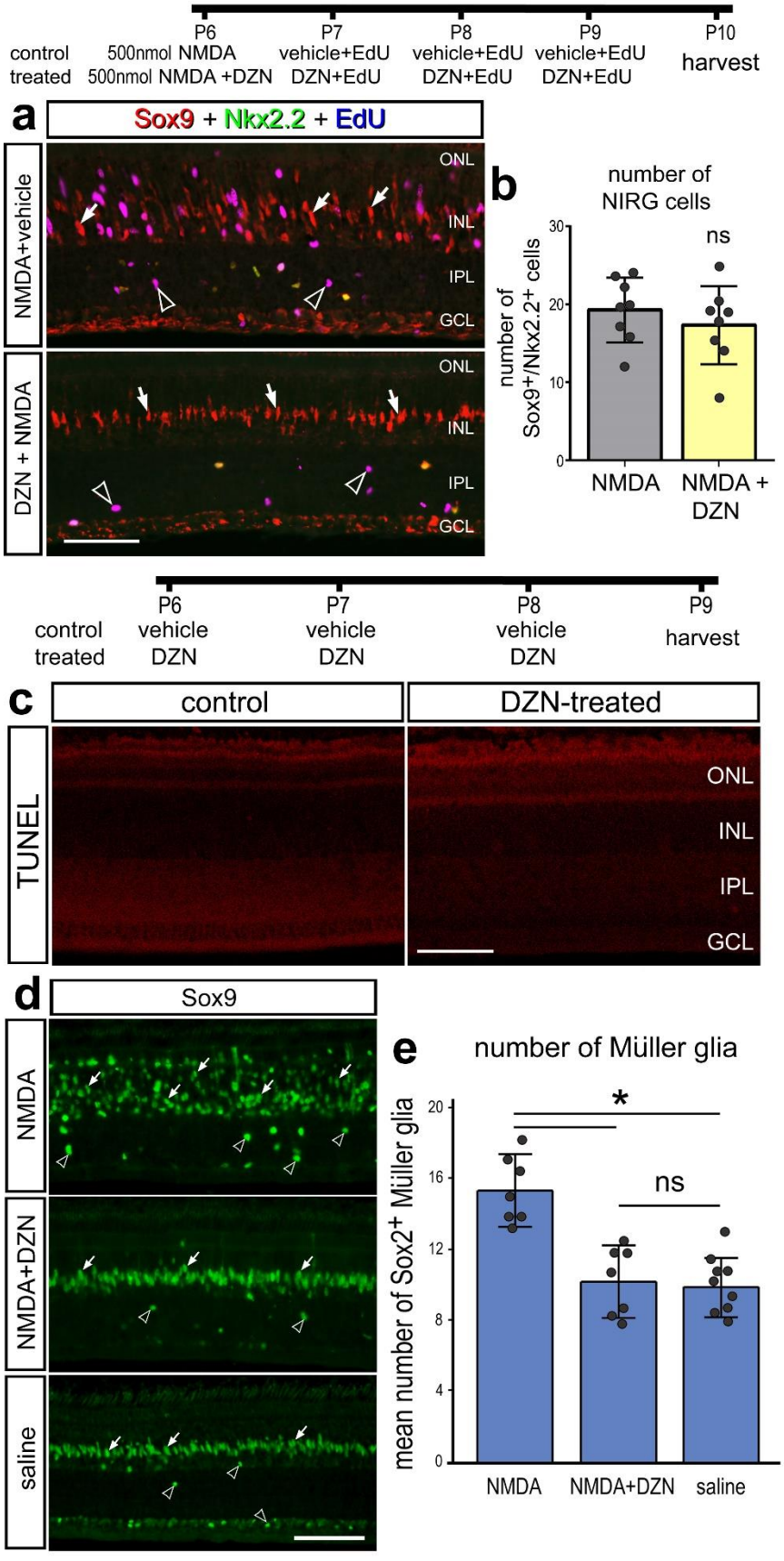

**Supplemental Figure 3. scRNA-seq in MG and MGPCs from different treatment paradigms.** scRNA-seq was used to identify patterns of expression of Jumanji-related genes in the at different time points after NMDA (**a,b**). UMAP clusters of MG (**c**) were identified by expression of cell-distinguishing genes resting MG (**c**), activated MG, and MGPCs (**d**). Each dot represents one cell and black dots indicate cells that express 2 or more genes. UMAP heatmap plots illustrate patterns and levels of expression of *JARID2*, *JMJD1C, JMJD4, JMJD5* and *JMJD6* (**e-g**). Violin/scatter plots indicate significant differences (*p<0.001, **p<1x10-10, ***p<1x10-20; Wilcox rank sum with Bonferoni correction) in expression levels of Jumanji-related genes in all retinal cells, MG/MGPCs and microglia (**h**).

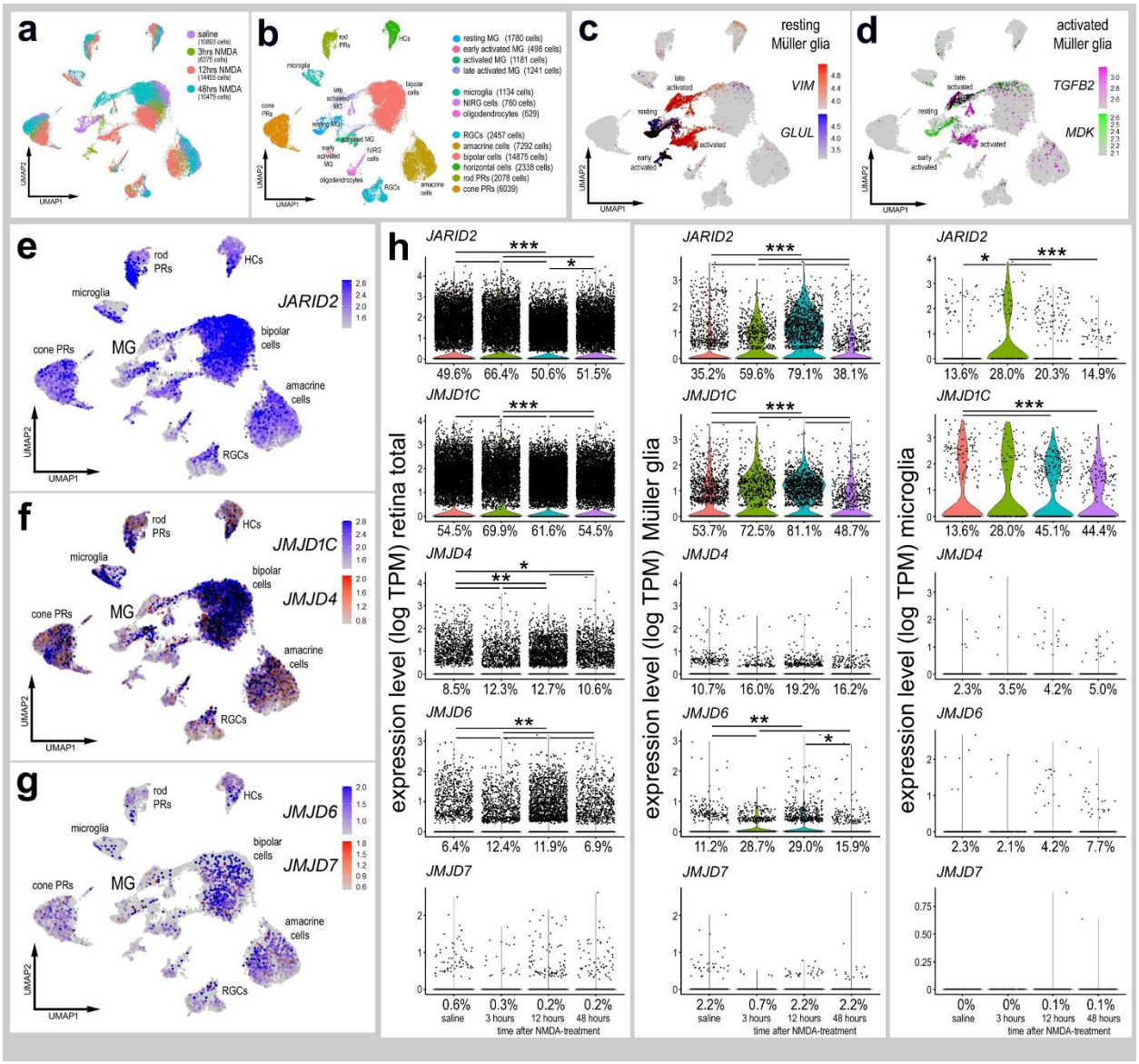

**Supplemental Figure 4. scRNA-seq analyses of MG in control retinas and retinas treated with NMDA, insulin and FGF2 or NMDA + insulin and FGF2.**

In UMAP and violin plots each dot represents one cell. MG were bioinformatically isolated from 2 biological replicates for control retinas and retinas treated with 2 doses of insulin and FGF2, 3 doses of insulin and FGF2, 24 hrs after NMDA, 48 hrs after NMDA, 48hrs after NMDA + insulin and FGF2, and 72 hrs after NMDA (**a**) UMAP analysis revealed distinct clusters of MG which includes control/resting MG, activated MG from retinas 24hrs after NMDA treatment, activated MG from 2 doses of insulin and FGF2, activated MG from 3 doses of insulin FGF2 and NMDA at different times after treatment, activated MG returning toward a resting phenotype from 48 and 72 hrs after NMDA-treatment, and 3 regions of MGPCs (**a-c**). The occupancy histogram in **b** illustrates the libraries of origin for cells in the different clusters of MGPCs. UMAP heatmaps illustrate elevated expression of *GLUL, RLBP, VIM* and *SLC1A3* in resting MG (**d**) and *CDK1, TOP2A, PCNA* and *SPC25* in different regions of MGPCs (**e**). UMAP and violin plots in **f-h** illustrate relative expression levels for *EZH2, EED, SET, RBBP4, JARDI2* and *AEBP2* in UMAP-clustered MG and MGPCs from different treatment groups. Significance of difference (*$p<0.001$, **$p<1x10^{-10}$, ***$p<1x10^{-20}$) was determined by using a Wilcox rank sum with Bonferoni correction. The number on each violin indicates the percentage of expressing cells.